The Plant Cell, Vol. 29: 1622–1641, July 2017, www.plantcell.org © 2017 ASPB.

Check for updates

Maize *YABBY* Genes *drooping leaf1* and *drooping leaf2* Regulate Plant Architecture[OPEN]

Josh Strable,[a,b,1,2] Jason G. Wallace,[c] Erica Unger-Wallace,[a] Sarah Briggs,[a] Peter J. Bradbury,[d] Edward S. Buckler,[d,e] and Erik Vollbrecht[a,b,2]

[a] Department of Genetics, Development and Cell Biology, Iowa State University, Ames, Iowa 50011
[b] Interdepartmental Plant Biology, Iowa State University, Ames, Iowa 50011
[c] Department of Crop and Soil Sciences, The University of Georgia, Athens, Georgia 30602
[d] U.S. Department of Agriculture–Agriculture Research Service, Ithaca, New York 14853
[e] Department of Plant Breeding and Genetics, Cornell University, Ithaca, New York 14853

ORCID IDs: 0000-0002-0260-8285 (J.S.); 0000-0002-8937-6543 (J.G.W.); 0000-0002-2248-9877 (E.U.-W.); 0000-0002-3100-371X (E.S.B.); 0000-0003-4919-1365 (E.V.)

Leaf architecture directly influences canopy structure, consequentially affecting yield. We discovered a maize (*Zea mays*) mutant with aberrant leaf architecture, which we named *drooping leaf1* (*drl1*). Pleiotropic mutations in *drl1* affect leaf length and width, leaf angle, and internode length and diameter. These phenotypes are enhanced by natural variation at the *drl2* enhancer locus, including reduced expression of the *drl2-Mo17* allele in the Mo17 inbred. A second *drl2* allele, produced by transposon mutagenesis, interacted synergistically with *drl1* mutants and reduced *drl2* transcript levels. The *drl* genes are required for proper leaf patterning, development and cell proliferation of leaf support tissues, and for restricting auricle expansion at the midrib. The paralogous loci encode maize CRABS CLAW co-orthologs in the YABBY family of transcriptional regulators. The *drl* genes are coexpressed in incipient and emergent leaf primordia at the shoot apex, but not in the vegetative meristem or stem. Genome-wide association studies using maize NAM-RIL (nested association mapping-recombinant inbred line) populations indicated that the *drl* loci reside within quantitative trait locus regions for leaf angle, leaf width, and internode length and identified rare single nucleotide polymorphisms with large phenotypic effects for the latter two traits. This study demonstrates that *drl* genes control the development of key agronomic traits in maize.

INTRODUCTION

Leaves maximize light capture and gas exchange across myriad environments and serve as the primary photosynthetic organ for almost all angiosperms. In natural and agricultural settings, leaves ultimately contribute to complex canopy architectures. For cereals like maize (*Zea mays*), canopy structure is a key component of optimal crop density (Pepper et al., 1977). Over the past century, breeders have mined diverse germplasms for alleles that alter leaf architecture traits, such as blade length, width, and angle, which are expressions of leaf patterning and collectively refine canopy structure. Modern maize commercial hybrids exhibit upright leaf architecture, a trait that maintains efficient light capture under denser planting practices (Duncan, 1971; Lambert and Johnston, 1978) and has led to significant gains in grain yield (Pendleton et al., 1968; Duvick, 2005). A fundamental question in plant developmental biology remains how leaf architecture is established and maintained during organogenesis.

The bifacial leaves of maize arise distichously (alternately in two vertical rows) as lateral primordia at the flank of the shoot apical meristem (SAM). Within the meristem, founder cells for the incipient leaf primordium are recruited in concert with those of the subtending internode and its associated axillary meristem (Sharman, 1942; McDaniel and Poethig, 1988). Together, these vegetative organs comprise a repeating unit of the shoot called a phytomer (Galinat, 1959), and the developmental interval of iterative, phytomer initiation is called a plastochron (Lamoreaux et al., 1978). Three discrete axes that define the mature maize leaf—proximal-distal, medial-lateral, and adaxial-abaxial—are established early and become apparent as the primordium emerges from the SAM periphery (Supplemental Figure 1; reviewed in Foster and Timmermans, 2009). Along the proximal-distal axis, the auricle and ligule define the boundary between the distal blade and proximal sheath. Functioning like a hinge, the mature auricle and ligule region contributes to canopy structure by angling the leaf and supporting midrib away from the stem. The medial-lateral axis is defined by the medial midvein and two lateral margins, with lateral veins running parallel between them (Sharman, 1942; Bosabalidis et al., 1994; Scanlon et al., 1996). Patterning along the adaxial-abaxial axis produces distinct epidermal characters, such as adaxial macrohairs and bulliform cells (Kiesselbach, 1949), and internal tissue arrangements such as polarized vascular bundles where xylem and phloem are positioned adaxially and abaxially, respectively (Russell and Evert, 1985).

Mutant studies in maize have identified many genes that pattern leaves, including several involved in or capable of affecting

[1] Current address: Section of Plant Biology, School of Integrated Plant Science, Cornell University, Ithaca, NY 14853.
[2] Address correspondence to jjs369@cornell.edu or vollbrec@iastate.edu. The authors responsible for distribution of materials integral to the findings presented in this article in accordance with the policy described in the Instructions for Authors (www.plantcell.org) are: Josh Strable (jjs369@cornell.edu) and Erik Vollbrecht (vollbrec@iastate.edu).
[OPEN] Articles can be viewed without a subscription.
www.plantcell.org/cgi/doi/10.1105/tpc.16.00477

Downloaded from https://academic.oup.com/plcell/article/29/7/1622/6099203 by U.S. Department of Justice user on 16 August 2022

establishment of the blade-sheath boundary (Foster and Timmermans, 2009). Recessive alleles of *liguleless1* (*lg1*; Becraft et al., 1990; Sylvester et al., 1990; Becraft and Freeling, 1991; Moreno et al., 1997) and *lg2* (Walsh et al., 1998) and the semidominant allele *Liguleless narrow-R* (*Lgn-R*; Moon et al., 2013) suppress development of ligule and auricle tissues, whereas in the semidominant allele *Liguleless3-O* (*Lg3-O*; Fowler and Freeling, 1996; Fowler et al., 1996; Muehlbauer et al., 1997), ligule and auricle are displaced distally along a prominent midrib. All four genes have been cloned (Moreno et al., 1997; Walsh et al., 1998; Muehlbauer et al., 1999; Moon et al., 2013); however, their downstream targets remain largely unknown. Due to their disrupted blade-sheath boundary, these mutants all have decreased leaf angle, i.e., more upright leaves, and therefore are associated with an altered canopy. Introgression of *lg2* mutant alleles in maize commercial hybrids resulted in an increase in yield (Pendleton et al., 1968; Lambert and Johnston, 1978). Furthermore, a genome-wide association study (GWAS) of leaf architecture in the maize nested association mapping (NAM) population, a diverse collection of ~5000 recombinant inbred lines (RILs) derived from 26 biparental families (McMullen et al., 2009), found significant quantitative trait loci (QTL) for upper leaf angle at the *lg1* and *lg2* loci (Tian et al., 2011).

The angiosperm-specific *YABBY* genes (Floyd and Bowman, 2007) play a significant role in leaf lamina development in *Arabidopsis thaliana* (Sawa et al., 1999; Siegfried et al., 1999; Goldshmidt et al., 2008; Sarojam et al., 2010), snapdragon (*Antirrhinum majus*) (Golz et al., 2004; Navarro et al., 2004; Stahle et al., 2009), and rice (*Oryza sativa*) (Nagasawa et al., 2003; Yamaguchi et al., 2004; Ohmori et al., 2011). In Arabidopsis, vegetative *YABBY* genes function redundantly to activate lamina developmental programs (Sarojam et al., 2010). In all flowering plants where *YABBY* expression has been investigated, *YABBY* transcripts are excluded from the central SAM, but accumulate in adjacent, emerging primordia, often asymmetrically: abaxially in eudicots (Sawa et al., 1999; Siegfried et al., 1999; Golz et al., 2004) and adaxially in maize (Juarez et al., 2004b). The rice *YABBY* gene *DROOPING LEAF* (*DL*), a member of the *CRABS CLAW* (*CRC*) clade (Yamaguchi et al., 2004), is expressed throughout incipient and emergent leaf primordia and is necessary for midrib development (Nagasawa et al., 2003; Yamaguchi et al., 2004; Ohmori et al., 2011). While it remains unclear how the *YABBY* genes function in maize during leaf development, *zea yabby9* (*zyb9*) and *zyb14* transcripts accumulate in lateral primordia in a pattern consistent with their association in establishing and/or maintaining leaf polarity (Juarez et al., 2004b).

Here, we report a mutant in maize we named *drooping leaf1* (*drl1*), a pleiotropic mutant highlighted by reduced midribs and distally extended auricles along the medial domain of the blade-sheath boundary. Importantly, both aspects contribute to the droopiness and increased angle of *drl1* mutant leaves. The *drl1* mutant phenotypes were drastically enhanced by the *drl2* locus in the Mo17 inbred line, the *drl2-Mo17* allele. We cloned the underlying genes and found that the paralogous loci encode maize CRC co-orthologs, putative transcriptional regulators with zinc-finger and YABBY domains. Our analyses suggest reduced expression of *drl2* in Mo17 likely enhances the *drl1* mutant phenotypes. A second *drl2* allele, produced by transposon mutagenesis, interacted synergistically with *drl1* mutants and substantially reduced *drl2* transcript levels. GWAS using the maize NAM-RIL populations revealed that the *drl* loci lie within QTL for leaf and stem traits and that the associations for leaf width and average internode length are rare but have large effects. Expression analyses demonstrate that *drl1* and *drl2* transcripts accumulate in lateral primordia, but not in vegetative meristems or developing stem. However, the *drl* genes influence meristem and stem traits, suggesting they may function non-cell autonomously. Our data reveal the important role of the maize *drl* genes in leaf and stem architectures.

RESULTS

The *drl* Genes Regulate Elaboration of the Phytomer

We identified *drl1-R*, the reference allele of *drl1*, as a spontaneous mutation in the B73 inbred background. Mutations in *drl1* were pleiotropic, with the most pronounced phenotypes on leaf (this study) and floral (J. Strable and E. Vollbrecht, personal observations) development, reminiscent of the rice *dl* mutant (Nagasawa et al., 2003; Yamaguchi et al., 2004). Given the pleiotropic nature of the *drl1-R* allele, it was backcrossed multiple generations into the A619, B73, Mo17, and W22 maize inbred lines to determine the most expressive phenotypes. We observed the effects of *drl1-R* on leaf architecture to be fully penetrant in all backgrounds; subsequently, we focused on B73 backcross and F2 introgressions for the majority of our study. Relative to the upright leaves of normal siblings, *drl1-R* leaves were noticeably droopy in both greenhouse- and field-grown plants (Figure 1A; Supplemental Figure 2). Leaf angle, defined in this study as the arc from the leaf midrib to the stem above it (Supplemental Figure 1), was markedly increased in *drl1-R* (Figures 1A, insets, and 1B). Also, leaf blades were significantly shorter and narrower in *drl1-R*; however, sheath lengths were increased (Figures 1C and 1D). In addition, *drl1-R* internodes were longer with reduced girth (Figures 1E and 1F). These data point to developmental roles for *drl1* in several elements of the phytomer.

Backcrossing *drl1-R* mutants to the Mo17 inbred line enhanced all aspects of the *drl1-R* phenotype (Figure 1; Supplemental Figure 2), where in a large F2 population we observed 249 enhanced *drl1-R* plants out of 3893 plants, consistent with an unlinked genetic modifier of *drl1-R* (15:1; $X^2 = 0.4$; P value > 0.5). We named this modifier *drl2-Mo17* because of its derivation (hereafter referred to as *drl2-M*) and, hence, the *drl1-R* enhanced individuals as *drl1-R; drl2-M* (see mapping below). To be consistent with our phenotypic analyses of *drl1-R*, we analyzed the *drl1-R; drl2-M* genotype within B73 introgression lines. We found leaf angle and stem diameter were most dramatically affected in *drl1-R; drl2-M* (Figures 1B and 1F). Additionally, *drl1-R; drl2-M* individuals displayed phenotypes not observed in the *drl1-R* single mutant. Leaf emergence rate was consistently slightly higher, such that at any time during seedling growth *drl1-R; drl2-M* individuals had at least one extra visible leaf relative to sibling plants (Supplemental Figures 3A to 3E). Vegetative phase change (Poethig, 2013) was also delayed slightly in *drl1-R; drl2-M* plants, which produced at least one extra juvenile leaf (Supplemental Figure 3A). At the blade-sheath boundary, *drl1-R; drl2-M* leaves displayed an enlarged auricle that was expanded medially to be continuous across the

Downloaded from https://academic.oup.com/plcell/article/29/7/1622/6099203 by U.S. Department of Justice user on 16 August 2022

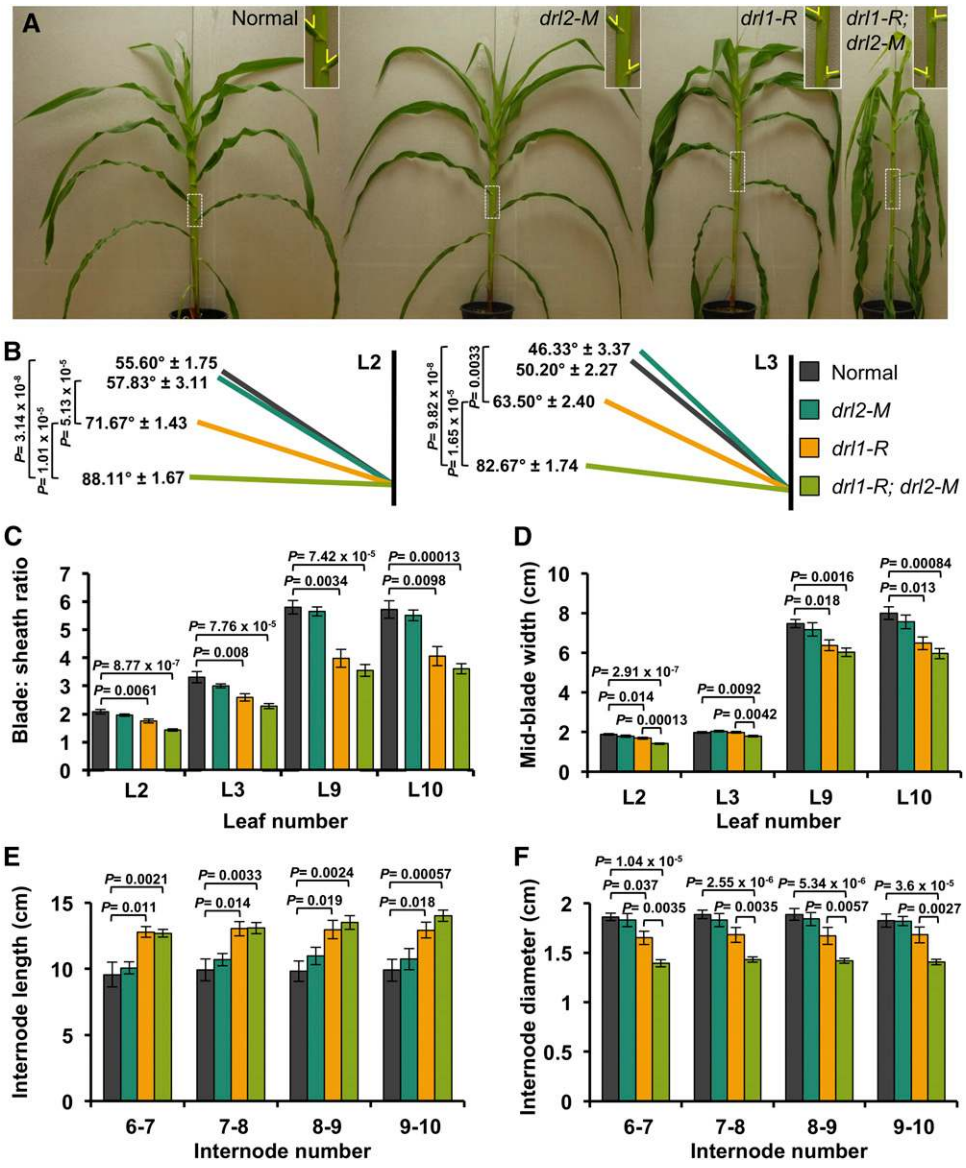

Figure 1. Leaf and Shoot Architecture of *drl1-R* and *drl1-R; drl2-M* Plants.

(A) to **(F)** Adult *drl1-R*, *drl2-M*, and *drl1-R*; *drl2-M* phenotypes in an F2-BC1 segregating family.
(A) General representation of *drl1-R* single mutants and mutants in the presence of the *drl2-M* modifier. Genotypes: normal (*drl1-R*/+; *drl2-M*/+), *drl2-M* (*drl1-R*/+; *drl2-M*), *drl1-R* (*drl1-R*; *drl2-M*/+), and *drl1-R*; *drl2-M* (*drl1-R*; *drl2-M*). Boxed regions of adult leaves (shown as insets) emphasize differences in leaf angle (yellow lines) at the blade-sheath boundary.
(B) Leaf angle for juvenile leaves 2 and 3; more upright leaves have smaller leaf angles, whereas droopy leaves have larger leaf angles.
(C) Ratio of total blade to sheath length for juvenile leaves 2 and 3 and adult leaves 9 and 10.
(D) Blade width taken at the midpoint of the blade for juvenile leaves 2 and 3 and adult leaves 9 and 10.
(E) Internode length for adult internodes 6-7, 7-8, 8-9, and 9-10.
(F) Internode diameter taken at the midpoint of the internode for adult internodes 6-7, 7-8, 8-9, and 9-10.
(B) to **(F)** Mean ± SE; P values based on two-tailed Student's *t* tests; $n = 5$ to 11.

midrib, as well as proximally, which gave it a collar-like appearance (Figure 2A, dotted lines; Supplemental Figures 3F and 3G). Occasionally at adult leaves, *drl1-R; drl2-M* margins were fused along the entire length of the sheath; for some individuals, this connate fusion persisted beyond the sheath into the auricle (Supplemental Figures 3H and 3I). Interestingly, on the first leaf of *drl1-R; drl2-M* plants, we consistently observed an ectopic outgrowth with sheath resemblance at the distal tip of the *drl1-R; drl2-M* mature blade (Supplemental Figures 3J to 3O). These spur-like outgrowths originated from the median plane of the blade.

Downloaded from https://academic.oup.com/plcell/article/29/7/1622/6099203 by U.S. Department of Justice user on 16 August 2022

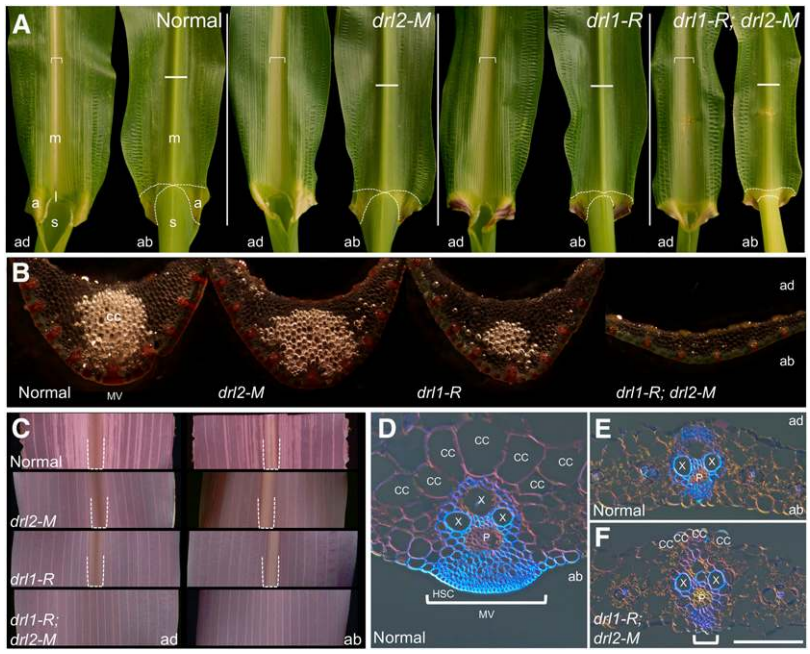

Figure 2. Morphology and Anatomy of *drl1-R* and *drl1-R; drl2* Leaves.

(A) Paradermal views of the adaxial (left) and abaxial (right) surfaces of adult leaf 8. Adaxial midrib cleft is denoted by a downward bracket. The horizontal line in abaxial view indicates the plate of the transverse section of the midrib shown in **(B)**. Abaxial auricle is outlined by dashed lines. All images are the same scale.

(B) Transverse, hand section of the distal midrib of adult leaf 8, taken 10 cm distal to the blade-sheath boundary and stained with Phloroglucinol-HCl.

(C) Paradermal views of adaxial and abaxial leaf 7 blade surfaces at the midpoint cleared and stained with eosin. Dashed brackets outline midrib region, which is absent in *drl1-R; drl2-M*.

(D) to **(F)** Transverse, microtome section of leaf 3 stained with Toluidine Blue-O.

(D) Normal midrib with midvein (upward solid bracket).

(E) Normal lamina with intermediate vein.

(F) Equivalent midrib region in *drl1-R; drl2-M* leaf with midvein (upward solid bracket).

ad, adaxial; ab, abaxial; a, auricle; b, blade; cc, clear cells, l, ligule; m, midrib; mv, midvein; p, phloem; s, sheath; hsc, hypodermal sclerenchyma cells; x, xylem. Bar = 200 μm.

Collectively, these data reveal that the *drl* genes regulate several key aspects of leaf patterning and shoot development.

The *drl* Genes Control Elaboration of Leaf Patterning along All Three Developmental Axes

To understand the cellular and structural basis of the *drl1* leaf phenotype, we performed histological and scanning electron microscopy analyses. In normal, mature leaves, the midrib runs along the medial plane of the blade as an adaxial indentation/abaxial ridge and often appears pale white, mostly because the tissue lacks chlorophyll-containing mesophyll cells. Midribs were broader, greener, and less defined in *drl1-R* and *drl1-R; drl2-M* leaves, particularly in *drl1-R; drl2-M*, where abaxial mesophyll cells were found throughout the medial domain (Figures 2A and 2B). These data, supported by observations that *drl1-R; drl2-M* vein spacing in the medial domain resembled lamina lateral veins (Figure 2C), indicate *drl* midribs have a more lamina-like identity.

Anatomically, the maize midrib consists of large clear cells positioned adaxial to the midvein (the median bundle) and lignified hypodermal sclerenchyma that connect to the abaxial epidermis (Figures 2B and 2D) (Sharman, 1942; Russell and Evert, 1985). In rice, *DL* gene activity in the medial region of leaf primordia (plastochrons 2 [P2]–P5) promotes extensive cell proliferation prior to the formation of the mature midrib (Yamaguchi et al., 2004; Ohmori et al., 2011). In distal transverse sections of the midrib, we observed a marked reduction in clear cell density in *drl1-R* mutants, with clear cells nearly absent in *drl1-R; drl2-M* individuals, which accounted for the overall less prominent, thinner midrib in the mutants (Figures 2B to 2F; Supplemental Figure 4). Similarly, in maize, the medial region of primordia thickens between P2 and P5 as cells proliferate (Supplemental Figures 4A3 and 4A4, yellow bar). This was not the case for *drl1-R* and *drl1-R; drl2-M* pre-midrib regions, where reduced cell proliferation across P2 to P5 primordia resulted in a thinner, less-defined medial region (Supplemental Figures 4C3, 4C4, 4D3, and 4D4, yellow bars). Furthermore, closer examination revealed that the lignified hypodermal sclerenchyma that is critical for support around the vascular bundle failed to develop fully and thus did not bridge the midvein and the abaxial epidermis in the *drl1-R; drl2-M* midrib (Figures 2D and 2F). Xylem and phloem polarity within the midvein bundle was normal in *drl1-R* and *drl1-R; drl2-M*, albeit the bundle was smaller, with

Downloaded from https://academic.oup.com/plcell/article/29/7/1622/6099203 by U.S. Department of Justice user on 16 August 2022

morphology that resembled lamina lateral veins (compared with Figures 2E and 2F). These data show that the *drl* genes establish the medial domain and elaborate lateral patterning, significantly contributing to leaf width. Importantly, the *drl* genes control leaf angle in part by regulating the development and proliferation of adaxial clear cells and abaxial hypodermal sclerenchyma in the midrib, critical support cell and tissue types along medial plane of the leaf blade.

Longitudinal sections of developing leaf primordia showed clear differences along the proximal-distal axis at the blade-sheath boundary. Mesophyll cell size within a developing leaf decreases proximally, such that blade cells are larger than auricle cells which are larger than sheath cells (Supplemental Figure 5A) (Becraft et al., 1990). In *drl1-R* primordia, however, auricle mesophyll cells were small relative to flanking blade or sheath cells (Supplemental Figure 5C). Moreover, mesophyll cells of the blade, auricle, and sheath were all uniformly small in *drl1-R; drl2-M*, and the adaxial-abaxial and proximal-distal planes were almost indistinguishable (Supplemental Figure 5D). Auricle tissue was expanded distally, which contributed to greater blade deflection (see below). Unlike mutants that displace the auricle, disrupt ligule, and show aberrant vascular anastomoses (Osmont et al., 2003; Foster et al., 2004; Hay and Hake, 2004), *drl1-R* and *drl1-R; drl2-M* ligules were continuous and lateral vein anastomosis patterns from the sheath into the blade were normal (Supplemental Figure 5E). These data reveal that the *drl* genes also regulate leaf architecture through elaborating proximal-distal patterning, though *drl* mutants do not have a grossly disrupted blade-sheath boundary.

At the blade-sheath boundary in normal leaves, the auricle is involuted in adaxial view, appearing slightly concave near the sheath margin where it connects the blade to the slightly narrower sheath (Figure 3A). In contrast, the curvature of *drl1-R* auricles was moderately reduced (Figure 3B), and *drl1-R; drl2-M* auricles appeared completely flat in the proximal-distal plane (Figure 3C). These reductions in auricle involution in the mutants could be attributed to the narrower leaf blades of *drl1-R* and *drl1-R; drl2-M*. Sheath width also decreased, with the *drl1-R; drl2-M* sheath appearing the narrowest (Figures 3A to 3C). These observations paralleled *drl1-R* blade width measurements (Figure 1D) and are consistent with trends in blade and sheath width data for other leaf mutants, such as *narrow sheath* (Scanlon et al., 1996) and *Lgn* (Moon et al., 2013).

In normal leaves, abaxial views revealed that the blade-sheath boundary was delineated along the proximal-distal axis by a uniform, slightly protruding ridge oriented perpendicular to the midrib (Figure 3D, arrowheads). This auricle-associated ridge was continuous from margin to margin and provides support at the blade-sheath junction. Epidermal cells in this ridge were evenly distributed, small, and uniformly round relative to the more elongated proximal sheath and distal blade epidermal cells (Figures 3D, white box, and 3G) (Becraft et al., 1990; Sylvester et al., 1990). Along the midrib, midvein hypodermal sclerenchyma had a greater contrast relative to a lesser contrast of blade and sheath epidermal cells; thus, the midvein appeared as a stripe that was continuous across the abaxial ridge (Figure 3D). Epidermal cells were less conspicuous in the *drl1-R* midrib region; the abaxial auricle ridge was more irregular and appeared diffused along the proximal distal axis of the auricle (Figure 3E, white box). Epidermal cells in the *drl1-R* abaxial auricle region, while smaller than neighboring sheath and blade cells, were not uniform in size or in distribution (Figure 3H). The *drl1-R; drl2-M* midrib region was nearly indistinguishable from neighboring lateral regions, as there was continuous spacing of lateral veins in the medial plane (Figure 3F). Additionally, the abaxial auricle ridge in *drl1-R; drl2-M* was completely reduced (Figure 3I). Auricle cell morphology in *drl1-R; drl2-M* was uniquely narrow, elongated, and often rugose (wrinkled; compared with Figures 3G and 3I), a distinct cellular topology that may reflect thickened and highly ordered microtubules in these elongated cells of expanded auricles (Yamamuro et al., 2000).

Taken together, our histology and scanning electron microscopy data demonstrate that the *drl* genes are required for proper patterning along all three axes of the maize leaf, for development and cell proliferation of support tissues in the maize leaf, and for restricting auricle expansion at the midrib. Thus, the *drl* genes are critical genetic factors that ultimately shape leaf architecture in maize.

The *drl* Genes Are the Maize *CRC* Co-Orthologs

Bulked segregant analysis (Michelmore et al., 1991) on 50 *drl1-R; drl2-M* individuals using a genome-wide SNP (single-nucleotide polymorphism) assay (Liu et al., 2010) showed linkage to markers IDP8570 and IDP1489 on the short arm of chromosome 1 and to IDP3975 and IDP7361 the long arm of chromosome 9 (Figures 4A and 4B). We used publicly available markers (Fu et al., 2005) to test 309 individuals (618 chromosomes per marker) for cosegregation. Fine mapping recombinant-sparse regions on chromosomes 1 and 9 identified the candidate genes *yabby2* (*yab2*; GRMZM2G088309) and *yab7* (GRMZM2G102218), respectively (Figure 4B) (Yilmaz et al., 2009; www.maizegdb.org), bolstered by the phenotypic similarity between *drl* and rice *dl* mutants. To determine the B73 or Mo17 origin of the *yab2* and *yab7* haplotypes, we used tightly linked markers IDP810 on chromosome 1 (for *yab2*) and IDP549 on chromosome 9 (for *yab7*). For IDP810, *drl1-R* single and *drl1-R; drl2-M* double individuals were homozygous for the B73 haplotype, whereas for IDP549, in *drl1-R* single individuals, both the B73 and Mo17 haplotypes segregated (Figure 4A). All *drl1-R; drl2-M* individuals were homozygous for the Mo17 haplotype using this chromosome 9 marker. These data indicate that the B73-dervied *drl1-R* is tightly linked to the *yab2* locus, whereas the *drl1-R* enhancer allele, *drl2-M*, is Mo17-derived and linked to the *yab7* locus.

We sequenced the *yab2* locus in normal, *drl1-R*, and *drl1-R; drl2-M* siblings and discovered a 2475-bp insertion within intron 6, located 24 bp upstream of the splice junction with exon 7 (Figure 4B). Except for three indels, this insertion matched exactly an insertion mutation in the *brown midrib1* gene (Chen et al., 2012); both insertion mutations were composed of segments of exact sequence matches to a region of the B73_RefGen_v3 sequence that encompasses the annotated transposon GRMZM2G017736. By requiring identical end points in all three cases, we determined that for each, the insertion is flanked by an 8-bp target site duplication as is typical of hAT family transposons in maize. The insertion at *yab2* (Figure 4B) was exclusive to the *drl1-R* allele and not present at the locus in the B73-derived progenitor

Downloaded from https://academic.oup.com/plcell/article/29/7/1622/6099203 by U.S. Department of Justice user on 16 August 2022

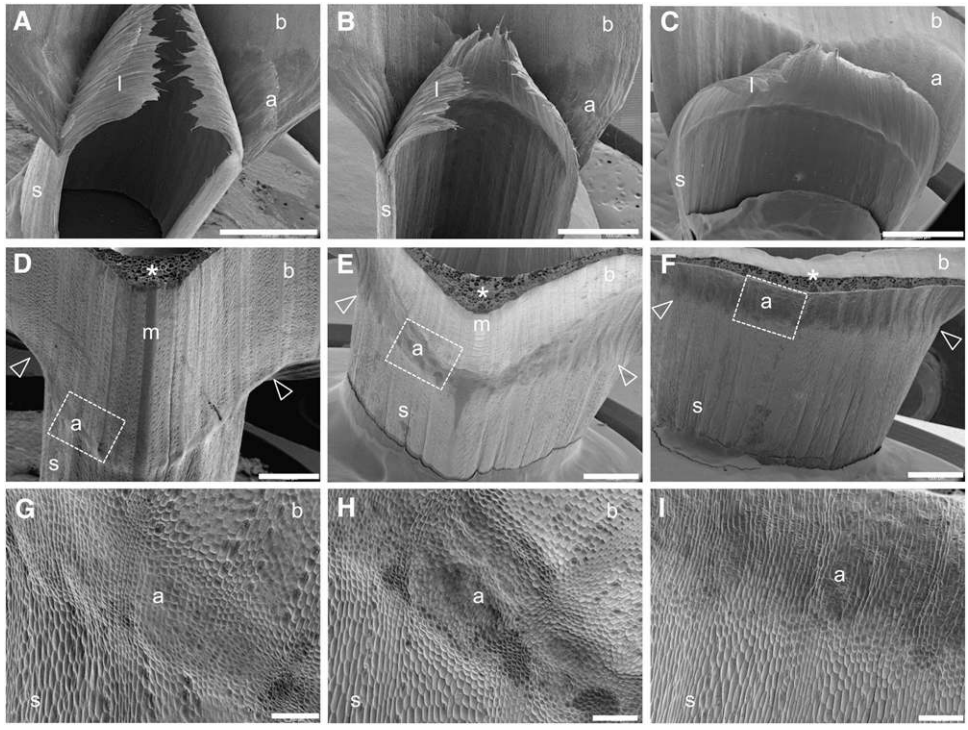

Figure 3. Morphology of *drl1-R* and *drl1-R; drl2-M* Blade-Sheath Boundary.

Scanning electron micrographs of adaxial (**[A]** to **[C]**) and abaxial (**[D]** to **[I]**) blade-sheath boundary of leaf 3. Boxed regions in **(D)** to **(F)** are enlarged in **(G)** to **(I)**, respectively. a, auricle; b, blade; l, ligule; m, midrib; s, sheath. Asterisk marks the midvein. Arrowheads denote auricle ridge. Bars = 2000 μm in **(A)** to **(C)**, 1000 μm in **(D)** to **(F)**, and 200 μm **(G)** to **(I)**.

(A), **(D)**, and **(G)** Normal.

(B), **(E)**, and **(H)** *drl1-R.*

(C), **(F)**, and **(I)** *drl1-R; drl2-M*.

chromosome, as determined by examining DNA from sibling and parental plants of the original isolate.

We generated a second *drl1* allele in the W22 inbred background using the *Activator* (*Ac*) and *Dissociation* (*Ds*) transposon system (Vollbrecht et al., 2010) by remobilizing a donor *Ds* element (B.S05.0371B) located 4.3 kb upstream of the annotated *yab2* transcription start site. We PCR-screened 1266 seedlings at the *yab2* locus and isolated a *Ds* insertion in exon 6 (*drl1-Ds*) (Figure 4B) that failed to complement *drl1-R* vegetative phenotypes (Supplemental Figure 6A). Backcrossing *drl1-Ds* into Mo17 inbred line resulted in enhancement of the *drl1-Ds* phenotype, consistent to what was observed for the *drl1-R* allele (Supplemental Figure 7). In the ear, *drl1-R* and *drl1-Ds* mutants had reduced carpel wall growth, unfused carpel walls and silks, and protruding nucelli (J. Strable and E. Vollbrecht, personal observations), reminiscent of the floral phenotypes described for the maize mutant *indeterminate floral apex1* (*ifa1*; Laudencia-Chingcuanco and Hake, 2002), for which no leaf phenotype has been reported. We therefore reexamined *ifa1* leaves and found they were droopy (Supplemental Figure 6D), which was enhanced by introgression of *ifa1* into the Mo17 inbred (Supplemental Figure 6E). Because the uncloned *ifa1* locus maps near *drl1* on chromosome 1S (Laudencia-Chingcuanco and Hake, 2002), we hypothesized that *ifa1* could be allelic to *drl1* and tested this through genetic complementation. In a cross between a *drl1-R*/+ heterozygote and an *ifa1* mutant, half of the F1 progeny displayed *drl1* leaf phenotypes; additionally, *ifa1* failed to complement *drl1-Ds* (Supplemental Figures 6B and 6C). We sequenced the *yab2* locus in *ifa1* mutants and discovered a single base-pair insertion in the 3′ splice acceptor site of the second exon/intron boundary (Figure 4B) that was not present in the maize HapMap2 data set (Chia et al., 2012; www.panzea.org; www.maizesequence.org). The *drl1-ifa* splice variant introduces a stop codon 22 amino acids downstream of the 3′ splice acceptor site (Supplemental Figure 8A). Overall, the lesions at *drl1*, identified in three independently isolated alleles, prove that *drl1* corresponds to the *yab2* gene.

We did not identify any putative lesions by sequencing the *yab7* locus in *drl1-R; drl2-M* individuals nor in the Mo17 inbred. We also searched in silico for predicted nonsynonymous nucleotide variation in the *yab7-Mo17* coding sequence relative to the B73 (nonenhancing) haplotype and found variation at two positions, encoding P167A and N205S (B73>Mo17) polymorphisms (Supplemental Figure 8B). Both were confirmed by sequencing the *drl2-M* allele and verified in the maize HapMap2 data set. However, these amino acid substitutions from nonsynonymous variation fall outside conserved regions in the DRL proteins (Supplemental Figure 8B) and are therefore expected to bear minimal, if any, effect on function. Similarly, in the *drl2-M* allele, the

Downloaded from https://academic.oup.com/plcell/article/29/7/1622/6099203 by U.S. Department of Justice user on 16 August 2022

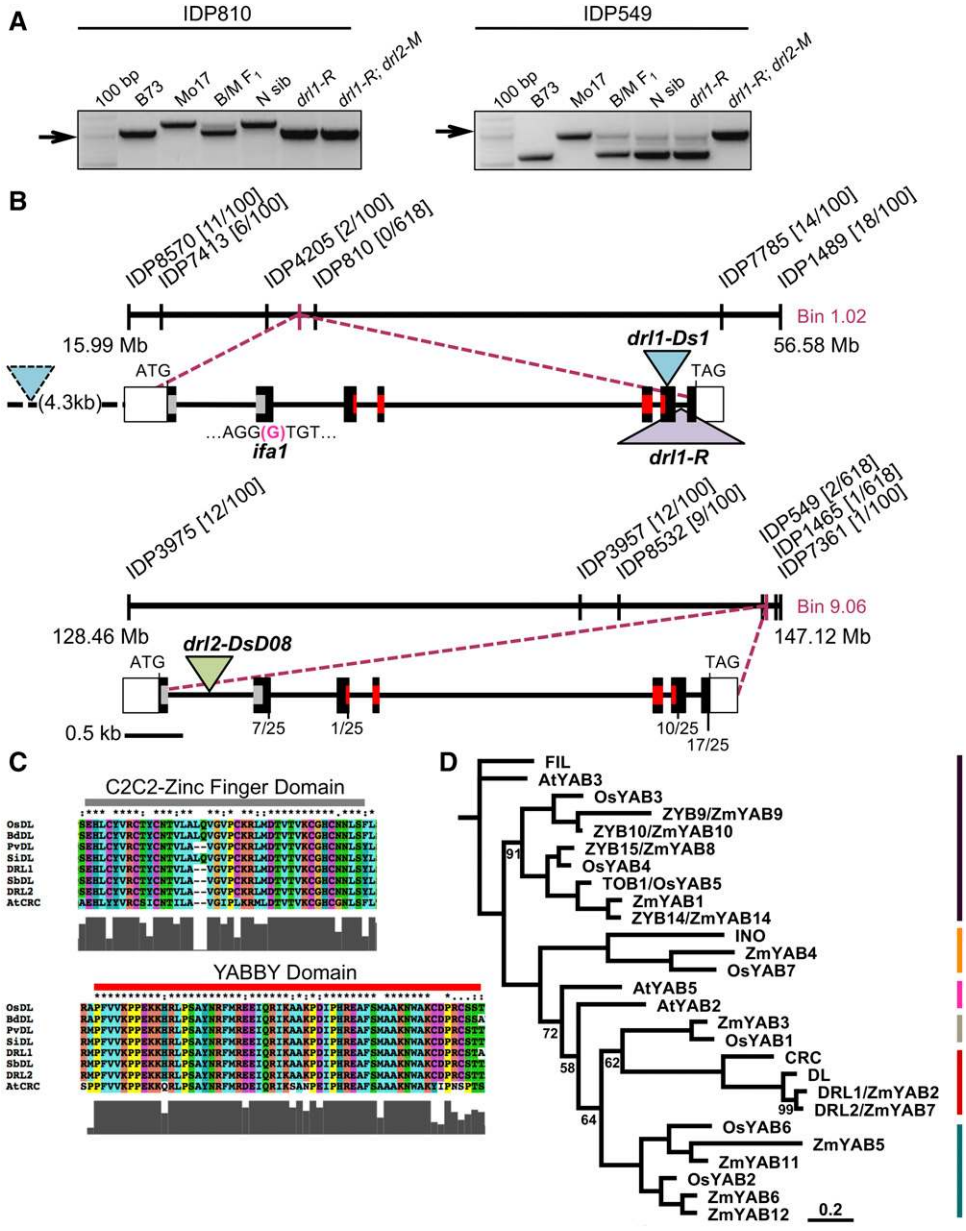

Figure 4. Positional Cloning, Gene Structure, and Phylogeny of *drl* and *drl2*.

(A) Genome-wide SNP assay showing segregation of indel codominant markers among individuals from the *drl1-R* (B73) × Mo17 F2 mapping population. IDP810, Ch1: 27,501,186-27,503,399 and IDP549, Ch9: 146,685437-146,688,265 (B73 RefGen_v2 assembly). Genomic DNA for inbred lines B73, Mo17, F1 progeny *drl1-R* (B73) × Mo17, F2 progeny for phenotypically normal, *drl1-R*, and *drl1-R; drl2-M* enhanced siblings. Arrow indicates the haplotype linked to the *drl1-R; drl2-M* enhanced sibling: B73 haplotype for IDP810 and Mo17 haplotype for IDP549. DNA ladder = 100 bp.

(B) Schematized summary of the positional cloning of *drl1* and identification of *drl2*. Two mapping interval regions are shown: ~40 Mb region for *drl1* on chromosome 1 (Bin 1.02) and ~20 Mb region for *drl2* on chromosome 9 (Bin 9.06). Recombinant chromosomes out of the total number of chromosomes screened are indicated above each marker. Gene structure of *yabby2* for *drl1* shows the location of the mutation for each of the three mutant alleles. Gene structure of *yabby7* for *drl2* shows the location of the *Ds* for the transposon mutant allele and the location and number of in silico predicted NAM founders with nonsynonymous nucleotide SNPs relative to B73. Open boxes, UTR regions; closed boxes, exons; gray, zinc-finger domain; red, YABBY domain.

(C) Amino acid alignment of the C_2C_2 Zinc Finger and YABBY domains across Pooid and Panicoid grasses and CRC from Arabidopsis.

(D) Bayesian phylogenetic analysis of all YABBY/CRC/DL-related proteins from Arabidopsis, rice, and maize. Posterior probability support is 100 at each node unless otherwise indicated. Vertical lines denote described clades: purple, FILAMENTOUS FLOWER (FIL) clade; yellow, INNER NO OUTER (INO) clade; red, CRC clade; fuchsia, gray, and teal lines represent lineages with limited functional analysis. Scale bar indicates number of expected changes per amino acid residue.

Downloaded from https://academic.oup.com/plcell/article/29/7/1622/6099203 by U.S. Department of Justice user on 16 August 2022

3′ untranslated region (UTR) contains a 24-bp insertion relative to B73, but the same polymorphism is present in the nonenhancing *drl2-P* allele (Supplemental Figure 9). We next evaluated expression of *yab7* in shoot apices of maize inbred lines B73, Mo17, and W22 and of *drl1-R* introgressions in those same backgrounds. We found measurable reduction of *yab7* expression in Mo17 apices relative to its expression in B73 apices (Supplemental Figure 9), suggesting that *drl2-M* enhancement of *drl1* alleles is reflected by *yab7* levels. Correspondingly, *yab7* expression was slightly reduced in W22 apices (Supplemental Figure 9), and we found that backcrossing the *drl1-R* allele into the W22 inbred line uncovered subtle enhancement of the *drl1-R* mutant phenotype (Supplemental Figure 2B). In W22, we observed graded enhancement of the *drl1-R* mutant phenotype in the *drl2-M*/*drl2-W* trans-heterozygous plants and strong enhancement in the *drl2-M* homozygous plants equivalent in severity to *drl2-M* enhancement in the B73 inbred (Supplemental Figure 2). Thus, allele-specific expression levels of *yab7* correlated with the effects of the *drl2* enhancer of *drl1* on leaf traits. To confirm that synergistic phenotypic interactions with *drl2-M* were due to genetic variation at the *yab7* locus, we used *Ds* transposon insertional mutagenesis (Li et al., 2013). Insertion of a *Ds* transposon in intron 2 of *yab7*, the *drl2-tdsgR22D08* allele (hereafter referred to as *drl2-DsD08*; Figure 4B), dramatically reduced *yab7* transcript levels relative to the progenitor allele from which *drl2-DsD08* arose (Supplemental Figure 9). Similarly, the *drl2-DsD08* allele enhanced all aspects of the *drl1-R* leaf phenotypes (Supplemental Figure 10), including the spur-like outgrowths on leaf 1, while the progenitor allele did not. Taken together, these results demonstrate that *drl2* is the *yab7* gene.

Reciprocal BLAST searches indicated that *drl1* and *drl2* encode transcriptional regulators homologous to the Arabidopsis *CRC* gene, the founding member of the *YABBY* family (Bowman and Smyth, 1999). In several eudicot and monocot species, *YABBY* genes modulate developmental programs in the lamina (Sawa et al., 1999; Siegfried et al., 1999; Nagasawa et al., 2003; Golz et al., 2004; Navarro et al., 2004; Yamaguchi et al., 2004; Goldshmidt et al., 2008; Stahle et al., 2009; Sarojam et al., 2010; Ohmori et al., 2011). An amino acid alignment of CRC-like proteins from Pooid grasses rice and *Brachypodium distachyon*, the Panicoid grasses *Panicum virgatum*, sorghum (*Sorghum bicolor*), foxtail millet (*Setaria italica*), and maize, and from Arabidopsis confirmed two highly conserved domains: an N-terminal C_2C_2 zinc-finger domain and a C-terminal helix-loop-helix YABBY domain, which shares sequence homology to the high mobility (HMG) box family of DNA binding proteins (Figure 4C) (Bowman and Smyth, 1999). Like what is observed for Arabidopsis and rice YABBY proteins, amino acids flanking the C_2C_2 zinc-finger and YABBY domains show the greatest degree of residue variation in maize (Supplemental Figure 8B).

Bayesian phylogenetic analysis on the 13 YABBY proteins from maize, the eight from rice (Toriba et al., 2007), and the six from Arabidopsis (Bowman and Smyth, 1999) placed the duplicate DRL1 and DRL2 proteins within a well-supported clade with the Arabidopsis CRC and rice DL proteins (Figure 4D; 1.00 posterior probability; Supplemental File 1). DRL1 (207 amino acids) and DRL2 (206 amino acids) proteins share 91.3% amino acid sequence identity (Supplemental Figure 8B). The *drl1* and *drl2* genomic regions are syntenically paralogous, while single *drl* syntenic orthologs of rice, Brachypodium, foxtail millet, and sorghum support the idea that the *drl1-drl2* duplicates arose during the maize tetraploidy event (Gaut and Doebley, 1997). For consistency based on community-accepted nomenclature for naming maize transcription factors (Gray et al., 2009; Yilmaz et al., 2009; www.maizegdb.org), we here refer to *zea yabby9* (*zyb9*), *zyb10*, *zyb14*, and *zyb15* (Juarez et al., 2004b) as *yab9*, *yab10*, *yab14*, and *yab8*, respectively (Figure 4D).

Conserved Noncoding Sequences Are Retained throughout the Maize *YABBY* Family

A conserved noncoding sequence (CNS) in the rice *DL* gene, shared in maize and sorghum orthologs, is critical for its temporal and spatial regulation during midrib development (Ohmori et al., 2011). We investigated the extent of CNSs across the maize *YABBY* family using VISTA footprint analysis (Supplemental Figure 11). Leveraging the sequenced genomes of many grasses (http://phytozome.jgi.doe.gov), we confirmed the critical CNS in intron 2 of rice and sorghum *DL* and maize *drl1* and *drl2* (Supplemental Figures 11B and 11G). We found that this CNS is also conserved in several additional grasses, including Pooid members Brachypodium, wheat (*Triticum aestivum*), and Panicoid members *P. virgatum*, *S. italica*, and *Setaria viridis*, and consists of two highly conserved nucleotide sub-blocks: one of 18 nucleotides (100% identity) and another of 65 nucleotides (83% identity) (Supplemental Figure 11N). It is tempting to speculate that disruption of this CNS in intron 2 in the *drl2-DsD08* allele is causative to the reduction in *yab7* expression and the subsequent enhancement of the *drl1* mutant phenotypes. We also found putative Panicoid-specific CNS regions, located in the maize genes *yab3* (intron 2), *yab5* (intron 1), *yab8* (intron 4), and *yab11* (intron 1, regions 1.1 and 1.2) (Supplemental Figures 11C, 11E, 11H, and 11K, respectively). Interestingly, a CNS that appears to be specific to maize, sorghum, *S. viridis*, and foxtail millet within the Panicoideae lies within *yab10* (intron 3; Supplemental Figure 11J). Thus, our analyses better resolve an existing CNS, including its possible mutation, and suggest CNS function may be common to multiple *YABBY* genes in the grasses.

Dose-Sensitive Interactions among the *drl* Genes

We observed synergistic genetic interactions between *drl1* mutant alleles and *drl2* Mo17 and W22 natural variant and mutant alleles. Because the *drl1* and *drl2* loci are coexpressed in overlapping domains, perhaps their function depends on gene product dosage, for example, through homo- or heterodimeric protein-protein or protein-CNS interaction, or both. Furthermore, in rice, a series of mutant *dl* alleles showed that graded activity of *DL* function correlates with phenotypic severity (Ohmori et al., 2008). We therefore hypothesized that *drl* activity would show dose-sensitive interactions. To examine *drl2*-independent dosage of *drl1*, we first self-crossed *drl1-Ds*/+ plants in a B73 background, i.e., in the absence of the Mo17 modifier allele at the *drl2* locus, and quantified leaf angles of genotyped F2 siblings. Leaf angle of *drl1-R* heterozygotes was in between that of the normal and *drl1-R* homozygotes (Figure 5A). To evaluate dosage of *drl1* in the presence of the *drl2-M* enhancer, we

Downloaded from https://academic.oup.com/plcell/article/29/7/1622/6099203 by U.S. Department of Justice user on 16 August 2022

quantified leaf angle among genotyped F2 progeny from a self-cross of *drl1-R*/+; *drl2-M*/+ plants. In combinations with *drl2-M* homozygotes, leaf angle of *drl1-R* heterozygotes was again intermediate between the normal and *drl1-R* homozygotes (Figure 5B). Similarly, relative to upright leaves of normal and *drl2-M* siblings, *drl1-R* leaves displayed moderate droopiness (Figures 5C to 5E), whereas *drl1-R; drl2-M*/+ leaves were droopier (Figure 5F) and *drl1-R; drl2-M* leaves displayed the droopiest phenotype (Figure 5G). Interestingly, although *drl2* expression is weak in Mo17 shoot apices relative to B73 apices, *drl2-M* (and *drl2-DsD08*) transcript levels were consistently further reduced in shoot apices of *drl1* mutants (Supplemental Figure 9). These results indicate a potentially complex interaction between *drl* alleles, including differing allele interactions between inbred lines. Furthermore, alleles of each *drl* locus exert dose-sensitive effects on leaf traits, suggesting that activity levels and/or interactions among gene products from the loci are important to their function.

The *drl* Genes Are Expressed Early in Leaf Primordia and Influence Meristem Size

The *drl* genes are necessary to specify structural cells and tissues of the midrib, such as clear cells and hypodermal sclerenchyma, and to promote their proliferation. To examine temporal and spatial patterns of *drl1* and *drl2* transcript accumulation during midrib, leaf, and shoot development, we performed RNA in situ hybridization. In median longitudinal and transverse sections through normal shoot apices, we detected *drl1* and *drl2* transcripts specifically in the medial region of the incipient (P0) and emergent (P1–P4) leaf primordia, but not in the SAM or adjacent developing internodes (Figures 6A to 6C and 6G to 6I) (Brooks et al., 2009; Ishikawa et al., 2009). Importantly, *drl1* and *drl2* transcripts were detected in precursors of adaxial clear cells and abaxial hypodermal sclerenchyma, cell types that are affected in the mature leaf by mutations in the *drl* genes, but not in the midvein provascular strand at P1-P2, which gives rise to cell types that are unaffected. To confirm that initiation of provascular development is unperturbed in *drl* mutants, we examined accumulation of the maize *PHABULOSA* ortholog (*ZmPHB*; Johnston et al., 2015), a class III homeodomain leucine zipper gene with well-described functions in adaxial patterning and vascular development (McConnell et al., 2001; Emery et al., 2003; Juarez et al., 2004a). We found comparable patterns of *ZmPHB* transcript accumulation in provascular strands in incipient and emerging leaf primordia of normal, *drl1-R*, and *drl1-R; drl2-M* apices (Supplemental Figures 12A to 12C). Within developing primordia, acropetal formation of the midvein provascular strand is correlated with differentiation of surrounding supportive tissues where *drl1* and *drl2* transcripts localize. This region of the primordium undergoes considerable adaxial thickening to form the midrib such that by P3, the emergent properties of the midrib are conspicuous (Sharman, 1942; Russell and Evert, 1985). Thus, the discrete expression patterns of *drl1* and *drl2* within developing leaf primordia correlate with establishment of the cell types and organs that are altered in the mutants.

In *drl2-M* apices, *drl1* transcripts were detected at levels comparable to their accumulation in B73 apices (Figure 6E). However, in *drl1-R* mutant apices, *drl1* transcripts were reduced and only detected at P0-P1 stages (Figure 6D); a similar reduction was observed in *drl1-R; drl2-M* apices (Figure 6F). Interestingly, accumulation of *drl2* transcripts was similarly reduced and only detected at P0-P1 stages in *drl2-M* apices (Figure 6K), but near normal levels were observed in primordia beyond P2 in *drl1-R* mutant apices (Figure 6J). The degree of *drl2* transcript accumulation in *drl2-M* apices was supported by RT-PCR, which showed reduced *drl2* transcript levels in *drl2-M* shoot apices (Supplemental Figure 9). Similarly, as was observed for *drl1*, accumulation of *drl2* transcripts in *drl1-R; drl2-M* apices was low and limited to P0 and P1 (Figure 6L). Thus, in either respective single homozygous or double homozygous class, we were unable to detect *drl1* or *drl2* transcripts consistently beyond P1, a critical stage in primordium development where sclerenchyma tissue and that of neighboring provascular tissue differentiate concomitantly. These data illustrate the critical timing and tissue specificity of *drl1* and *drl2* expression during the early stages of midrib development.

We found the vegetative shoot apices of *drl1-R*, *drl2-M*, and *drl1-R; drl2-M* to be consistently smaller than B73 apices, even though *drl* transcripts were not detected in the SAM proper (Figure 6). This observation was based on comparing the distance between *drl* transcript accumulation in the P0 and the crown of the SAM. To confirm that reduced meristem size corresponded to the distance between *drl* transcript accumulation and the SAM crown, we examined the expression of the maize ortholog of *CUP-SHAPED COTYLEDON2* (*CUC2*). In maize, *CUC2* is a robust marker of the boundary between leaf primordia and the SAM as early as P0 (Johnston et al., 2014, 2015). *CUC2* expression was detected above the incipient primordium (P0), at the boundaries between emergent primordia and the SAM (P1-P2), and in the boundaries between older primordia and the stem (>P3) (Supplemental Figures 12D to 12F). *CUC2* transcripts also accumulated in the disc of insertion at the incipient phytomer node (D0) and at nodes of older plastochrons (D1–D4) (Supplemental Figures 12D to 12F) (Johnston et al., 2015). Thus, *CUC2* and *drl* expression patterns at P0 were complementary (compare Figures 6A and 6D with Supplemental Figures 12D to 12F). *CUC2* transcript accumulation in *drl1-R* and *drl1-R; drl2-M* vegetative shoot apices supports our observation that the vegetative meristem in these mutants is reduced in size. Taken together, the expression pattern of *drl1* and *drl2* and the consistent reduction in meristem size in the *drl* mutants suggests the *drl* genes may function non-cell autonomously.

The *drl* Loci Reside within Quantitative Trait Regions for Leaf and Stem Traits

Maize contains considerable natural variation for shoot architecture traits (Tian et al., 2011; Peiffer et al., 2013, 2014). We found that the *drl* loci play an important qualitative role in determining leaf and stem architectures, that natural allelic variation at *drl2* imparts quantitative variation on the *drl1* mutant phenotype, and more generally that alleles of each *drl* locus exert dose-sensitive, quantitative effects on leaf phenotypes. We therefore investigated whether *drl1* and *drl2* colocalize with QTL for maize developmental traits that have agronomic significance. For this, we used the maize NAM population, a massive and diverse germplasm resource (McMullen et al., 2009). The NAM population was constructed by

Downloaded from https://academic.oup.com/plcell/article/29/7/1622/6099203 by U.S. Department of Justice user on 16 August 2022

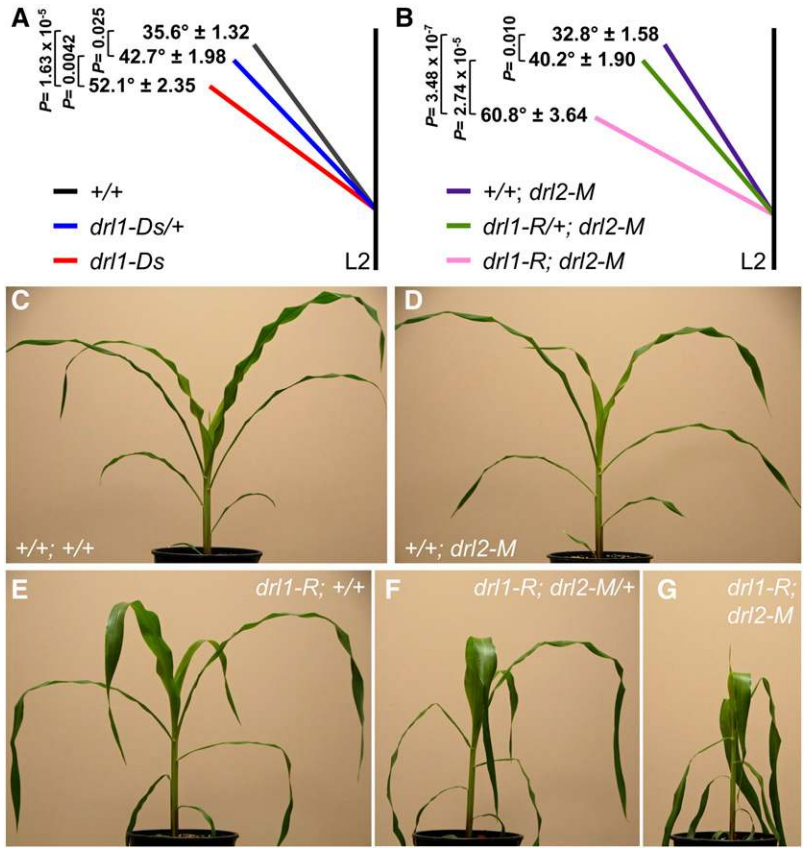

Figure 5. Dosage Effects of *drl1* and *drl2* on Leaf Phenotypes.

(A) Leaf angle for juvenile leaf 2 from an F2 population of +/+ (n = 10), *drl1-Ds*/+ (n = 20), and *drl1-Ds*/*drl1-Ds* (n = 16).
(B) Leaf angle for juvenile leaf 2 from an F2 population of +/+; *drl2-M* (n = 12), *drl1-R*/+; *drl2-M* (n = 19), and *drl1-R*; *drl2-M* (n = 6).
(C) to **(G)** Vegetative phenotype from a segregating F2 population. Dosage effects on leaf traits were observed by fixing the *drl1-R* allele and varying the dosage at *drl2-M*.
(A) and **(B)** Mean ± SE; P values based on two-tailed Student's t tests.

crossing the reference B73 inbred line with 25 diverse founder inbred lines; subsequently, from each of these F1 families, 200 recombinant inbred lines were generated by self-pollinating (McMullen et al., 2009). We leveraged phenotypic data generated previously using the maize NAM population (Buckler et al., 2009; Tian et al., 2011; Peiffer et al., 2014) to perform high-resolution GWAS on 12 diverse shoot phenotypes (Supplemental Table 1).

To identify regions on chromosomes 1 and 9 controlling variation in leaf and stem architectures, we tested the association of 6.9 million segregating polymorphisms from maize HapMap1 (Gore et al., 2009) and HapMap2 (Chia et al., 2012). These polymorphisms in the NAM founder lines were projected onto the 5000 RIL progeny using pedigree and linkage marker information based on low-density markers generated by genotyping-by-sequencing (Elshire et al., 2011; Wallace et al., 2014a). We performed a forward-regression GWAS to identify genetic variants that associated with the various shoot phenotypes (Kump et al., 2011; Poland et al., 2011; Tian et al., 2011; Peiffer et al., 2013, 2014; Wallace et al., 2014a; Zhang et al., 2015). Briefly, our forward-regression model iteratively scanned a subset of the genome, chromosomes 1 and 9, and with each run only the most robust SNP was added to the model until no significant SNPs remained. To obtain a robust association, such analysis was repeated 100 times for each trait, with a random 80% of each family subsampled each iteration. To gauge the strength and stability of the associations, polymorphisms were filtered based on their resample model inclusion probability (RMIP) (Valdar et al., 2009), meaning the frequency that they were chosen by the model. The RMIP value ranges from 0 to 1; we chose a RMIP cutoff of at least 0.05, or five runs out of 100. Significant SNPs (RMIPs ≥ 0.05) were identified by GWAS close to or within the *drl* loci (Figure 7). Other significant SNPs were also identified at a greater distance from each gene, although linkage disequilibrium (LD) analysis indicated that rare SNPs could be spreading signal across one megabase or more around these genes (Supplemental Figures 13A and 13B).

We observed significant association of SNPs for leaf width and leaf angle at the *drl1* locus (Figures 7A and 7B, respectively). For leaf width, GWAS detected two significant SNPs (RMIPs 0.05 and 0.07) within the annotated *drl1* intron 4 (Supplemental Data Set 1). These GWAS hits were rare, appearing only in the CML333 and

Downloaded from https://academic.oup.com/plcell/article/29/7/1622/6099203 by U.S. Department of Justice user on 16 August 2022

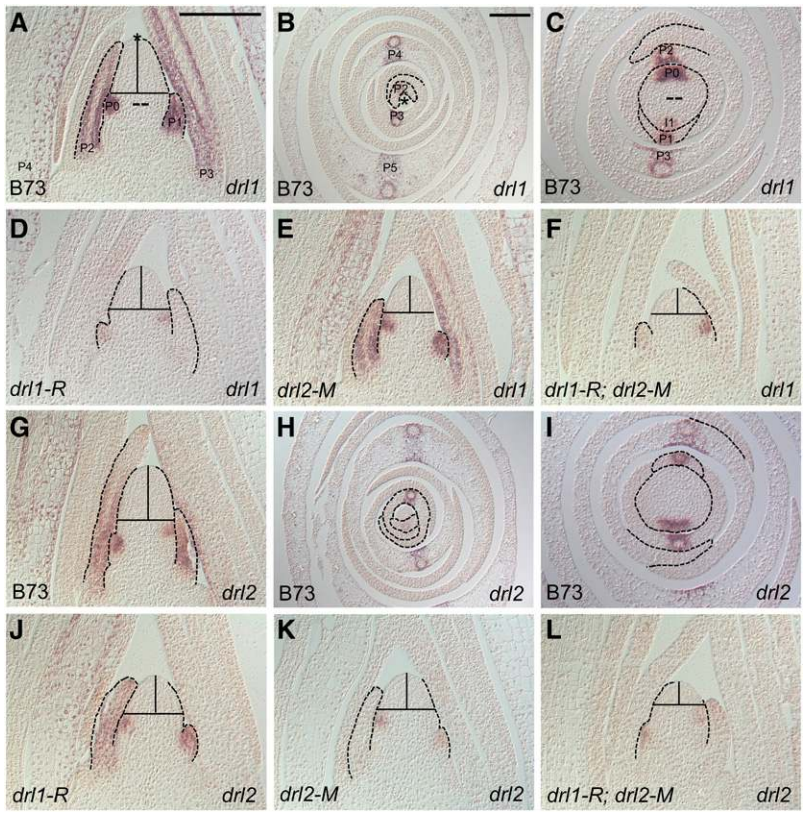

Figure 6. RNA in Situ Hybridization of the Shoot Apices of *drl1* and *drl2*.

Median longitudinal sections through shoot apices from B73 (**[A]** and [**G**]). Transverse sections through B73 shoot apices at the tip of (**[B]** and **[H]**) and within (**[C]** and **[I]**) the meristem. Median longitudinal sections through shoot apices from *drl2-M* (**[E]** and **[K]**), *drl1-R* (**[D]** and [**J**]), and *drl1-R; drl2-M* (**[F]** and **[L]**). Antisense probes for *drl1* (**[A]** to **[F]**) and *drl2* (**[G]** to **[L]**). All apices were 2.5 weeks old. *drl1* transcripts accumulate strongly in P0-P4 leaf primordia in B73 **(A)** and *drl2-M* **(E)** shoot apices; however, transcript accumulation is reduced to only P0 and P1 in *drl1-R* **(D)** and *drl1-R; drl2-M* **(F)** shoot apices. *drl2* transcripts accumulate strongly in P0-P4 leaf primordia in B73 **(G)** and *drl1-R* **(J)** shoot apices; however, transcript accumulation is reduced to only P0 and P1 in *drl2-M* **(K)** and *drl1-R; drl2-M* **(L)** shoot apices. Transverse sections of B73 shoot apices above (**[B]** and **[H]**) and within (**[C]** and **[I]**) the shoot apical meristem show strong transcript accumulation in P0-P4 leaf primordia. Note: For all shoot apices, transcripts are not detected throughout the meristem, subtending stem, or midvein provascular tissue. Dashed outlines denote the leaf primordia. Asterisk marks the tip of the meristem. Double dash marks within the meristem. Bar = 200 μm.

M37W NAM founder lines and had among the largest effects (+2 mm in width) relative to SNPs throughout the entire genome (Figure 7E). Despite their large effects, these SNPs explained little variance for this trait in the population (Supplemental Figure 13C) due to their rarity. For leaf angle, GWAS detected a significant polymorphism (RMIP = 0.1) ~2.5 kb upstream of the *drl1* locus. This GWAS hit was relatively common, occurring in 10 NAM founder lines (Supplemental Data Set 1), was of small effect (Figure 7F), and explained little variance (Supplemental Figure 13D). The two *drl1* intronic associations for leaf width and the single *drl1* promoter association for leaf angle were derived from different haplotypes, indicating that QTLs for these traits were likely not shared. This result is consistent with the findings of Tian et al. (2011), who detected very little pleiotropy for various leaf traits. For the *drl2* locus, GWAS detected three significant SNP associations for average internode length; however, the bulk of this QTL's signal appeared to reside upstream of the locus (Figure 7C). Two of these GWAS hits were rare: one (RMIP = 0.03) was found downstream of the locus in the Il14H, Mo17, and NC350 NAM founder lines and was of strong effect (−1 to −1.5 mm; Figure 7G). The other hit (RMIP = 0.07) was found in intron 5 in HP301, Il14H, M37W, and NC350 and was of modest effect size (−1 mm; Figure 7G). The third GWAS hit (RMIP = 0.01) for average internode length was also found in intron 5 for seven NAM founder lines (Supplemental Data Set 1) and was of small effect (Figure 7G). We found that *drl2* resided in a poorly resolved QTL for leaf angle (Figure 7D), and SNPs in the locus proximity had small phenotypic effects (Figure 7H). These data demonstrate that natural variation in maize breeding lines at the *drl* loci affects various aspects of leaf and stem architectures, agronomically important yield traits.

Maize GWASs detected minimal contribution of epistatic interactions to overall trait effects (Buckler et al., 2009; Tian et al., 2011; Zhang et al., 2015), though the epistatic effects might be too small to detect or may only minimally contribute to the overall trait effect (Wallace et al., 2014b). We tested for digenic (two-locus) effects among leaf architecture QTL (see Methods) and did not

Downloaded from https://academic.oup.com/plcell/article/29/7/1622/6099203 by U.S. Department of Justice user on 16 August 2022

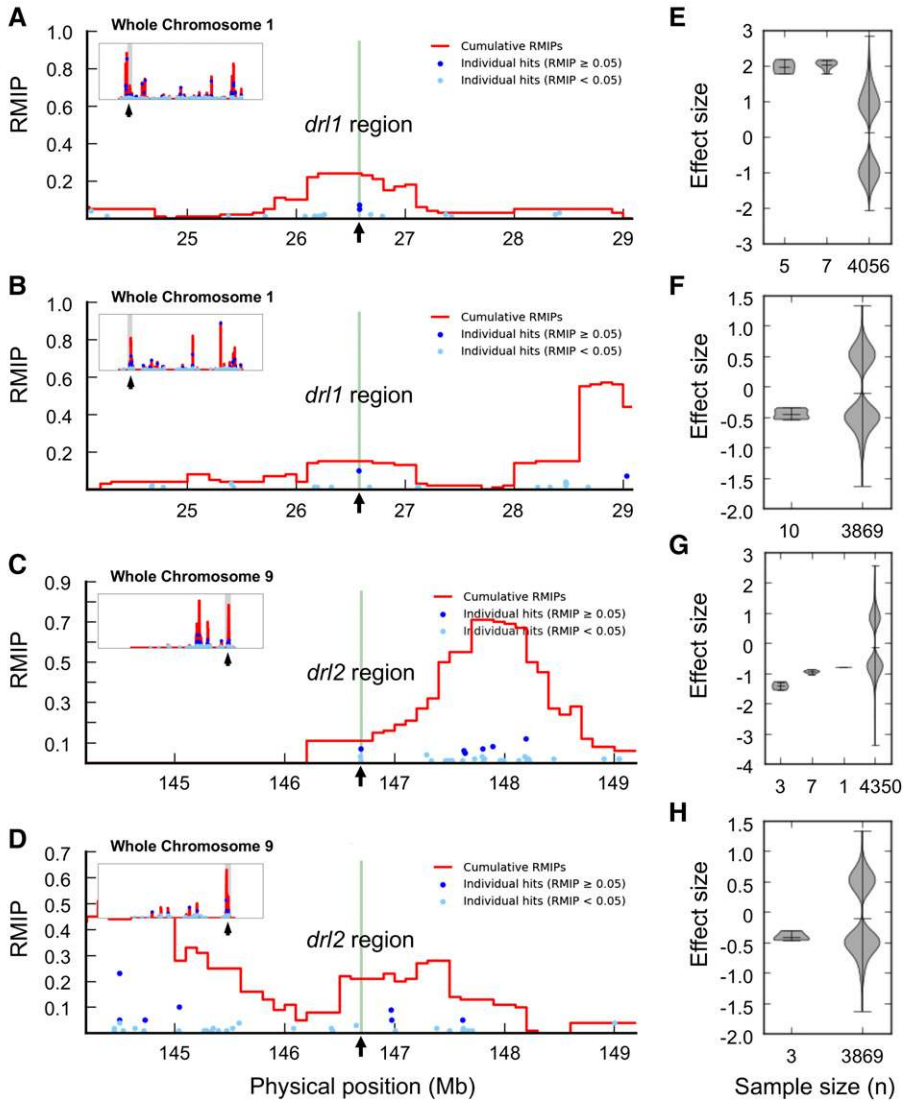

Figure 7. QTL and Phenotypic Effect Sizes of GWAS Hits at the *drl* Loci in the NAM Population.

(A) to **(D)** Potential QTL were identified around the *drl1* and *drl2* loci (green line and arrow in the center of each plot) on chromosomes 1 and 9, respectively, using previously published maize GWAS data. Individual points show GWAS hits: Dark-blue dots indicate higher quality hits that have an RMIP ≥0.05; light-blue dots indicate lower quality hits that are less well resolved. The red lines show the cumulative RMIP in 1-Mb sliding windows. Inset: whole chromosomal view with arrows at the *drl1* or *drl2* locus.

(A) to **(D)** *drl1* leaf width **(A)**, *drl1* Boxcox-transformed leaf angle **(B)**, *drl2* average internode length across the whole plant **(C)**, and *drl2* Boxcox-transformed leaf angle **(D)**.

(E) to **(H)** The effect size for each SNP located in *drl1* or *drl2* was determined across all HapMap2 GWAS models that included it (out of 100 bootstrapped iterations). The sample size for the violin plots is the number of times a variant was selected as part of the model, and the violins represent the distributions for different variants in each *drl* gene. The distributions are shown for individual SNPs at left. The large, rightmost bimodal distribution in each violin plot shows the effects for all SNPs across all models, i.e., all variants selected combined across all 100 model iterations. The plot is bimodal because SNPs with effect sizes near 0 are rarely selected by the model, effectively filtering them out.

(E) and **(F)** *drl1* shows one of the largest effect sizes for leaf width (approximately +2 mm) **(E)** and small effect sizes for leaf angle (Boxcox transformed) **(F)**. **(G)** and **(H)** *drl2* shows strong effects for average internode length (approximately −1.5 mm) **(G)** and small effect sizes for leaf angle (Boxcox transformed) **(H)**.

Downloaded from https://academic.oup.com/plcell/article/29/7/1622/6099203 by U.S. Department of Justice user on 16 August 2022

identify any significant digenic epistatic interactions between associations (Supplemental Figure 14). These data suggest that among the leaf architecture QTLs we detected around the *drl* loci, the epistasis effects are unimportant or very minor in controlling leaf traits. Alternatively, because of the low diversity at *drl1*, the NAM alleles that may associate with it are rare; hence, any epistatic interactions with it will also be infrequent, to the point that it may not be possible to identify them with this data set.

DISCUSSION

Leaf architecture is a major determinant of yield in maize (Pendleton et al., 1968; Duncan, 1971; Lambert and Johnston, 1978; Duvick, 2005; Tian et al., 2011). During the last century, maize breeders have selected for sheath and blade lengths, blade widths, and leaf angles that optimize light capture under high planting density. Altering cell specification and differentiation programs during leaf development has great potential to improve leaf architecture. In *drl1* single mutants, important leaf traits are altered: Sheaths are elongated, auricles are distally expanded, blades are shorter and narrower, midribs are less defined, and leaf angles are reduced. Genetic combinations of *drl1* mutant alleles with the *drl2* natural variant and mutant alleles enhance all phenotypes of *drl1* single mutants (Figures 1 to 3; Supplemental Figures 2 to 5) in a dose-dependent manner (Figure 5) and reveal phenotypes not observed in *drl* single mutants (Supplemental Figure 3). The *drl* genes play key roles in regulating leaf architecture, and overall plant architecture, in diverse maize breeding lines (Figure 7).

Primordia-Derived Activities of *drl* Genes Regulate Shoot Meristem Growth

Like the rice *DL* locus, the maize *drl1* and *drl2* loci encode CRC-like transcription factors (Figure 4D). *CRC*, the founding member of the *YABBY* gene family, was first characterized in Arabidopsis from mutants with altered carpel development (Alvarez and Smyth, 1999; Bowman and Smyth, 1999). The *CRC* homolog *DL* was the first *YABBY* gene to be described in rice (Nagasawa et al., 2003; Yamaguchi et al., 2004). Subsequently, functions of other *YABBY* members have been described in Arabidopsis (Chen et al., 1999; Sawa et al., 1999; Siegfried et al., 1999), *Antirrhinum majus* (Golz et al., 2004), and rice (Tanaka et al., 2012), and their expression patterns have been reported in maize (Juarez et al., 2004b). Genetic and expression analyses of the *YABBY* genes in eudicots have implicated their cell autonomous role in specifying abaxial cell fate in the leaf (Bowman and Smyth, 1999; Sawa et al., 1999; Siegfried et al., 1999; Golz et al., 2004). More recent studies using reporter lines, and loss- and gain-of-function alleles suggest *YABBY* genes are also involved in non-cell-autonomous communication between developing primordia and meristems to regulate meristem activity, although the mechanism by which this communication is achieved remains unknown (Eshed et al., 2004; Golz et al., 2004; Goldshmidt et al., 2008; Stahle et al., 2009; Sarojam et al., 2010; Tanaka et al., 2012). Here, we report several non-cell-autonomous effects for the maize *drl* genes. *drl1* and *drl2* transcripts are excluded from the SAM proper and subtending stem (Figure 6), yet *drl* mutants are affected in meristem size (Figure 6; Supplemental Figure 12), internode length and diameter (Figure 1), the production of axillary meristems (J. Strable and E. Vollbrecht, personal observations), leaf initiation rate, and phase change (Supplemental Figure 3). Thus, beyond just the leaf per se, all elements of the phytomer are affected. Several reports align with the hypothesis that signals expressed in the primordia act to control the meristem. Early experimentation in pea (*Pisum sativum*) showed that a leaf-derived signal influences leaf initiation rate and growth (Snow, 1929). Shoot culture studies in maize demonstrated that signals limiting vegetative growth and those that define phase change are intrinsic to the primordium and, through a non-autonomous signal derived from leaves, act at the shoot apex (Irish and Nelson, 1988; Irish and Jegla, 1997; Irish and Karlen, 1998). The non-cell-autonomous properties of ADT, the product of an enzyme encoded by the maize gene *bladekiller1*, which acts in the thiamine biosynthesis pathway, is important for maintaining meristem indeterminacy (Woodward et al., 2010). FASCIATED EAR3, a key regulator of stem cell proliferation in maize, responds to the FON2-LIKE CLE PROTEIN1 peptide signal produced in lateral organ primordia (Je et al., 2016). Our results are consistent with and reinforce the standing hypothesis in the research field on *YABBY* function (Goldshmidt et al., 2008; Stahle et al., 2009; Sarojam et al., 2010; Tanaka et al., 2012): The maize *drl* gene products act in or through pathways that function non-cell autonomously, which traverse boundary domains or peripheral layers of the primordium to regulate developmental programs at the shoot apex.

Spatial regulation of brassinosteroids (BRs) is required for proper development of lateral organs and regulation of organ boundary formation (Clouse and Sasse, 1998; Clouse, 2011; Wang et al., 2012). BRs influence leaf bending and internode elongation in maize (Hartwig et al., 2011; Makarevitch et al., 2012; Kir et al., 2015) and rice (Wada et al., 1981; Cao and Chen, 1993; Yamamuro et al., 2000; Hong et al., 2002; Zhang et al., 2009; Tong et al., 2012; Tsuda et al., 2014; Sun et al., 2015), regulate adaxial cell elongation in auricles (Wada et al., 1981; Cao and Chen, 1993), reduce abaxial sclerenchyma proliferation (Sun et al., 2015) in rice, and cause organ fusion in Arabidopsis (Bell et al., 2012; Gendron et al., 2012). Our findings indicate that the *drl* genes regulate a suite of traits in the leaf and stem similar to those affected by BR; however, a connection between these two important developmental regulators has not been established. *drl1* mutant alleles together with *drl2* natural variant and mutant alleles condition a phenotype that strongly resembles aspects of rice mutants that have elevated BR levels or enhanced BR signaling (Zhang et al., 2009; Tong et al., 2012; Tsuda et al., 2014; Sun et al., 2015): *drl* mutants have narrow leaves, increased leaf angle, expanded auricles, reduced sclerenchyma, and elongated internodes (Figures 1 to 3; Supplemental Figure 3). One peculiar phenotype observed in *drl1-R; drl2-M* plants was complete fusion along the sheath margins at some adult nodes Supplemental Figure 3l), a phenotype related to BR hypersensitivity in Arabidopsis (Bell et al., 2012; Gendron et al., 2012). Given these observations, we speculate that within developing primordia and organ boundaries, BR, acting as a local morphogenic signal, could potentially mediate *drl* activity during lateral organ development. Developing knockout resources to generate higher-order mutant combinations will help to test this hypothesis.

Downloaded from https://academic.oup.com/plcell/article/29/7/1622/6099203 by U.S. Department of Justice user on 16 August 2022

drl Dose-Sensitive Interactions Shape Leaf Architecture

Whole-genome duplication generates duplicate loci, including their associated regulatory sequences (Bennetzen and Freeling, 1993; Moore et al., 1995; Schnable et al., 2011). Gene fractionation, or gene loss, of syntenic paralogs relieves the genome of costs associated with maintaining redundancy; however, when gene products of paralogs contribute to dose-sensitive interactions, selection pressure exists for their retention (reviewed in Freeling, 2009). Retention is imposed by at least two functional constraints: dose-sensitive protein-protein interactions, where subunit stoichiometry is critical, and dose-sensitive protein-DNA interaction, where balance between dose-sensitive transcription factors, their *trans*-DNA targets, and their own *cis*-regulatory regions may be essential, especially when those *cis* regions contain CNSs (Schnable et al., 2011; Schnable, 2015). The *drl* genes are syntenic paralogs, coexpressed in overlapping domains in developing primordia (Figure 6). We found CNSs throughout the maize *YABBY* family, with those in the *drl* loci most deeply conserved (Supplemental Figure 11). Furthermore, we found that *drl1* and *drl2* displayed dose-sensitive genetic interactions (Figure 5). Such genetic interactions could be due to a critical balance established by multimeric protein-protein or protein-DNA interactions, or both. In Arabidopsis, YABBY proteins can form homodimers and heterodimers (Stahle et al., 2009), and the proteins likely participate in multiprotein regulatory complexes (Boter et al., 2015). Our study demonstrates that maize *drl* genes exert dose-sensitive effects on leaf traits early in their development, suggesting that levels or thresholds of *drl* gene products are critical to their function.

Quantitative Variation in the *drl* Loci Influences Leaf and Stem Architectures

Mutations in *drl1* altered leaf and stem architectures, and these phenotypes were enhanced by the *drl2-M* allele. We considered the *drl* loci to be candidates for leaf and stem QTL and examined them for enriched proximity to previously published GWAS SNPs for leaf and stem traits. We identified polymorphisms within QTL intervals for *drl1* and *drl2* that are associated with variation for leaf and internode traits (Figure 7). Importantly, our GWAS identified rare SNPs with large phenotypic effects for leaf width and average internode length (Figures 7E and 7G). A few millimeters are not a large proportion of the total width of the leaf, yet the effects of *drl1* on size are among the largest effects on leaf width identified in this population (Figure 7). Natural variants have previously been shown to have much more modest effects than induced mutants (Peiffer et al., 2014), probably because large effects are more likely to be deleterious and thus purged by natural selection. Overall, polymorphisms contributing to variation for these traits were tightly linked to the *drl* loci, occurring in promoter, genic, or immediate downstream regions. The SNPs we identified potentially lie close to or even are a causal polymorphism due to the statistical power gained in NAM, since empirically most LD in NAM decays below background levels within 1 kb of any given polymorphism (Supplemental Figures 13A and 13B) (McMullen et al., 2009; Wallace et al., 2014a). Recent work in maize indicates that variation in gene regulation and copy number is more likely a frequent driver of functional variation and influence on quantitative traits than differences in protein coding sequences that alter protein function (Wallace et al., 2014a). Indeed, Wallace et al. (2014a) found that genes identified by GWAS often show enrichment for genetic variation in regulatory regions. Genetic variants found by GWAS are likely to be paralogous (duplicated) genes, suggesting that phenotypic variation is largely driven by gene duplication and by regulatory divergence (Wallace et al., 2014a). Maize paralogs with *cis*-acting protein binding sequences, such as the CNSs we identified in the *drl* genes, are more likely to be retained following tetraploidy than paralogs that lack CNSs (Schnable et al., 2011). Our study on the *drl1* and *drl2* paralogs complements these findings and further demonstrates their agronomic potential to regulate leaf and stem architectures, important agronomic traits that directly affect yield. Furthermore, this study illustrates the potential impact in future breeding efforts to improve plant architecture through mining allelic variation at the *drl* loci, especially if surveys of larger populations (e.g., the Ames Inbred Diversity Panel; Romay et al., 2013) reveal alleles with stronger effects.

METHODS

Origin of the *drl1-R* Allele and Genetic Stocks

The *drl1-R* maize (*Zea mays*) allele arose spontaneously, in a stock where the *ramosa1-63.3359* allele (http://www.maizegdb.org/data_center/stock?id=259221) had been introgressed into the B73 (*ra1-63* B73-8) background. *drl1-R* was isolated in an F2 population from an F1, *drl1-R*/+; *ra1-63*; B73-8/Mo17-6 individual that was self-pollinated. This population segregated two phenotypes: *drl1-R* and a *drl1-R enhanced*, with the latter at a 15:1 ratio. Mapping of the *drl1-R enhanced* phenotype located both *drl1-R* and a natural variant locus from the Mo17 inbred line, the *drl1* paralog *drl2*. The *drl1-R* allele was backcrossed to A619, B73, Mo17, and W22 inbred lines at least three times. The *ifa1* (B73-4) allele was obtained from Sarah Hake (UC Berkeley). Given our detailed description of mutant, vegetative phenotypes associated with both paralogs, we use *drl1* to refer to its various pseudonyms in maize (GRMZM2G088309, *drooping leaf ortholog1* [*dlo1*] or maize *DROOPING LEAF1* [*ZmDL1*] [www.maizegdb.org], *ifa1* [Laudencia-Chingcuanco and Hake, 2002] and *yab2* [Yilmaz et al., 2009; www.grassius.org]) and *drl2* to refer to its various pseudonyms in maize (GRMZM2G102218, *dlo2* and *ZmDL2* [www.maizegdb.org], and *yab7* [Yilmaz et al., 2009; www.grassius.org]). The *drl2-tdsgR22D08* allele was generated as part of the Li et al. (2013) study and was obtained from the Maize Genetic Coop Stock Center. The *Ac*/*Ds* material used to generate the *drl1-Ds* allele is also available from the Maize Genetics Coop, as stock AcDs-00668 (Vollbrecht et al., 2010).

Positional Cloning of *drl1-R* and Identification of *drl2-M*

Several F2 mapping populations were generated from F1 self-pollinations of a *drl1-R*/+; *ra1-63*; B73-8/Mo17-6 individual. These populations segregated two phenotypes: *drl1-R* at a 3:1 ratio and a *drl1-R enhanced* at a 15:1 ratio; mapping was performed exclusively within the *drl1-R enhanced* class. Genetic linkages were established on a pool of 50 *drl1-R enhanced* individuals (compared with 50 normal individuals) to the short arm of chromosome 1 (bin 1.02) and the long arm of chromosome 9 (bin 9.06) using a combination of bulked segregant analysis (Michelmore et al., 1991) and Sequenome-based SNP-typing assays (Liu et al., 2010). We used publically available insertion/deletion polymorphisms between the B73 and Mo17 inbred lines (Fu et al., 2005) to narrow candidate regions by fine mapping on an expanded population of 314 *drl1-R enhanced* individuals. The candidate *drl1-R yabby2* locus was PCR amplified and sequenced in the B73 and Mo17 inbred lines and in normal, *drl1-R*, and

Downloaded from https://academic.oup.com/plcell/article/29/7/1622/6099203 by U.S. Department of Justice user on 16 August 2022

drl1-R enhanced individual siblings. The candidate *drl2 yabby7* exons were PCR amplified and sequence in the B73 and Mo17 inbred lines and in normal, *drl1-R*, and *drl1-R enhanced* individual siblings.

Isolation of *drl1-Ds*

The *drl1-Ds* allele was isolated from populations generated by testcrossing female maize plants (W22 inbred, *r1-sc:m3* allele) without *Ac* transposase with male maize plants carrying the *Ds* donor B.S05.0371B (http://www.acdstagging.org/v2/generate.php?id=B.S05.0371B) and *Ac-immobilized*. A total of 1266 purple and spotted testcross kernels were screened in the greenhouse. A single one-eighth-inch disc of leaf tissue was harvested from the first visible leaf from each plant ~10 d after sowing. The tissue from eight individual plants was combined in a single tube. Genomic DNA was isolated from tissue pools using a method described previously (Gao et al., 2010) with slight modification. A second centrifugation (3000*g* for 10 min) was added to clear the cell lysates further prior to loading onto 96-well glass fiber filter plates (Corning 3511). DNA was eluted from plates in 200 μL water, and 2 μL was used as template for PCR. A remobilization event of the B.S05.0371B element was detected using a three-primer strategy. PCR was performed under standard conditions using GoTaq Green Master Mix (Promega) with 5% DMSO (v/v) plus two *Ds*-specific primers and one *drl1*-specific primer or two *drl1*-specific primers plus one *Ds*-specific primer (Supplemental Table 2). Amplification followed standard conditions, and amplicons were resolved using agarose gel electrophoresis. Pools that contained a putative *Ds* insertion were deconvoluted to a single plant using the same DNA isolation methods described above, except that two discs of leaf tissue were taken from the second visible leaf from each of the eight plants that comprised a single pool. When a *Ds* amplicon was isolated from a single plant, Sanger sequencing of the amplicon using the *Ds* end primer determined the exact location of the new insert, and the plant was transplanted and grown to maturity to recover the *drl1-Ds* allele through pollinations.

Histology

Eosin staining was performed on fully expanded adult leaf 7. Eosin was dissolved in 100% ethanol to make a 1% staining solution (w/v). Leaf blades and auricles were cleared in 3 parts glacial acetic acid to 1 part ethanol (v/v) at room temperature with multiple changes until the tissue was clear. Tissues were then rinsed several times in distilled water and stained with a 1% eosin staining solution overnight at room temperature. The samples were then rinsed in 70% ethanol for several changes to destain.

Toluidine Blue-O (TBO) (Sigma-Aldrich) staining was performed on 2-week-old shoot apices. Briefly, TBO was dissolved in 1% sodium borate (w/v) to make a 1% stock solution (w/v). A 0.5% TBO staining solution was made immediately before use by diluting the stock solution with 1% sodium borate and mixing well. Microtome sections of 10 μm, adhered to a microscope slide, were deparaffinized in Histo-Clear (National Diagnostics) (two times, 10 min each). Slides were passed through a graded ethanol series toward hydration, 1 min each (100%, 100, 95, 95, 70, 50, distilled water) and stained in 0.5% TBO staining solution for 10 min. Slides were then passed through a graded ethanol series toward dehydration, 20 s each (50%, 70, 95, 95, 100, 100) and Histo-Clear (three times, 5 min each). Slides were dried briefly and cover slip mounted with Permount (Fisher).

Phloroglucinol-HCl staining was performed as described previously (Tang et al., 2014) with slight modifications. Briefly, midribs from adult leaf 8 were hand-sectioned 10 cm from the ligule using a double-edge razor. Phloroglucinol-HCl (Sigma-Aldrich) was dissolved in 95% ethanol to make a 2% stock solution. A 1% Phloroglucinol-HCl staining solution was made immediately before use by diluting the stock solution with concentrated hydrochloric acid (33%, v/v) and mixing well. Midrib sections were immersed in the 1% Phloroglucinol-HCl staining solution for 5 min, placed on a glass microscope slide with residual Phloroglucinol-HCl stain, and imaged immediately under a stereomicroscope (Leica MZ125). Light images were captured using a digital camera (Canon EOS Rebel XSi).

Scanning Electron Microscopy

Greenhouse grown leaves 2 and 3 were fixed with 2% paraformaldehyde and 2% glutaraldehyde in cacodylate buffer (0.1 M) at pH 7.2 for at least 24 h/4°C. After fixation, the samples were rinsed three times (15 min each) in cacodylate buffer (0.1 M). The samples were then postfixed in 1% osmium tetroxide in cacodylate buffer (0.1 M) for 1 h. After several washes with deionized water, the samples were dehydrated through a graded ethanol series (25%, 50, 70, 85, 95, 100), two changes each for 15 min. The samples were critical point dried using a model DCP-1 drying apparatus (Denton Vacuum). Dried materials were mounted on aluminum stubs with double-sided tape and colloidal silver paint and sputter coated with gold-palladium with a Denton Desk II sputter coater (Denton Vacuum). Images were captured using a JEOL JSM-5800LV scanning electron microscope at 10 kV.

RNA in Situ Hybridization and Expression Analysis

Shoot apices from 2.5-week-old seedlings were fixed overnight at 4°C in 3.7% FAA. The samples were dehydrated through a graded ethanol series (50%, 70, 85, 95, 100) each 1 h, with two changes in 100% ethanol. The samples were then passed through a graded Histo-Clear (National Diagnostics) series (3:1, 1:1, 1:3 ethanol:Histo-Clear) with three changes in 100% Histo-Clear; all changes were 1 h each. The samples were then embedded in Paraplast Plus (McCormick Scientific), sectioned, and hybridized per Javelle et al. (2011). The *drl1* and *drl2* CDSs are 93% identical, whereas their predicted 3′ UTRs are ~66% identical. Antisense probes were generated by PCR amplification of cDNA with the goal of capturing stretches of unique sequence between the *drl* paralogs. Two fragments for *drl1* consisted of 585 bp that spanned exons 2 and 7 (drl1_F1 + drl1_R7; 88% identical with *drl2*) and 300 bp that spanned exon 7 and the 3′ UTR (drl1_F8 + drl1_R4; 73% identical with *drl2*), and two fragments for *drl2* that consisted of 603 bp that spanned exons 1 and 7 (drl2_F17 + drl2_R11; 93% identical with *drl1*) and 369 bp that spanned exon 5 and the 3′ UTR (drl2_F11 + drl2_R9; 79% identical with *drl1*). Except in some cases with shared sequence identity between the *drl* probes, probe specificity for highly homologous genes in the shoot apical meristem has been demonstrated previously by in situ hybridization (Jackson et al., 1994). Fragments were subcloned into pCR 4-TOPO (Invitrogen) and confirmed by Sanger sequencing. Antisense digoxygenin-UTP labeled RNA was generated for *drl1* and *drl2* using a DIG RNA labeling kit (Roche). For *drl1* hybridizations, equal amounts of the two probes for *drl1* were mixed prior to hybridization. Similarly for *drl2* hybridizations, equal amounts of the two probes for *drl2* were mixed prior to hybridization. Primer sequences for in situ probes are provided in Supplemental Table 2.

Shoot apices from 1-month-old seedlings were dissected and placed individually in 600 μL Trizol (Thermo-Fisher) and stored at −80°C until processing. Five 3-mm tungsten carbide beads (Qiagen) were added and the samples ground for 30 s in a Genogrinder (Spex SamplePrep). The grindates were transferred to a new tube and incubated at room temperature for 10 min, followed by centrifugation at 4°C for 10 min. The supernatants were diluted with an equal volume of ethanol, and total RNA was prepared using Direct-zol RNA miniPrep (including DNase-I treatment; Zymo Research). cDNA was generated from 4 μg of total RNA using RNA to cDNA EcoDry Premix (Double Primed) reagents (Takara Bio USA). The cDNA was diluted 1:1 with water, and 1.0 μL was used for PCR. *Yab2* (drl1_F8 + drl1_R4), *yab7* (EUO1128 + EUO1131), and *ubiquitin* (Ubi_F1 + Ubi_R1) PCR followed standard conditions using GoTaq Green Master Mix (Promega), annealing temperature = 60°C, 1 min extension at 72°C for 31 and 35 cycles. Primer sequences are listed in Supplemental Table 2.

Downloaded from https://academic.oup.com/plcell/article/29/7/1622/6099203 by U.S. Department of Justice user on 16 August 2022

Phylogenetic Analysis

Protein sequences for DRL1 and its Pooid, Panicoid, and Arabidopsis orthologs were aligned using ClustalX (Jeanmougin et al., 1998) for the following sequences: OsDL (LOC_Os03g11600), BdDL (Bradi1g69900.1), PvDL (Pavirv00051928), SiDL (Si037608), SbDL (Sb01g042850), and AtCRC (AT1G69180). Protein sequences of the 13 maize, eight rice (*Oryza sativa*), and six *Arabidopsis thaliana* YABBY family members (see Accession Numbers), obtained by BLAST searches of protein databases from www.maizesequence.org, www.phytozome.net/, and www.arabidopsis.org, were aligned using the MAFFT multiple sequence alignment program (Katoh and Toh, 2010). The resulting alignment file was used to infer a phylogenetic tree using MrBayes v3.2.3 (Huelsenbeck and Ronquist, 2001) with the mixed amino acid probability model. Mr. Bayes was run for three million generations, a sample frequency of 100, and burn-in value of 10,000. The phylogeny was rooted with AtFIL sequence as an outgroup.

Phylogenetic footprinting was performed at Phytozome 10.3 (http://phytozome.jgi.doe.gov) using VISTA (Frazer et al., 2004) annotations available on Jbrowse (Skinner et al., 2009).

GWAS in the NAM Population

GWAS hits in the maize NAM population (McMullen et al., 2009) using HapMap2 genotypes (Chia et al., 2012) were taken from an existing study (Wallace et al., 2014a). QTL regions were determined by summing the RMIP (Valdar et al., 2009) in 1-Mb sliding windows with a 100-kb step size.

Variance Explained

The variance explained by each SNP was determined by fitting a linear model for each trait per the following formula:

$$y = \mu + family + snpi..j + family : snpi..j,$$

where "y" is the vector of phenotypes, "μ" is the population mean, "family" is a vector of family terms (one each for the 25 NAM families), "$snp_{i..j}$" are the vectors of genotype values for each SNP in the model, and "family: $snp_{i..j}$" is the interaction between the family term and each SNP. (That is, each SNP is allowed to have a different effect in each family.) Genotypes were scored as 0 (B73 allele) or 1 (non-B73 allele), with heterozygous and imputed genotypes scored as decimal values between these.

Linkage Disequilibrium

LD was calculated by identifying all SNPs within 1 Mb of *drl1* and *drl2* and calculating the pairwise linkage disequilibrium (Pearson's r^2) between them and each nonredundant SNP within the genes. ("Redundant" SNPs are those with identical genotypes across all lines; only one SNP out of every such set was used for LD calculation to prevent overweighting specific haplotypes.)

Test for Epistasis

Epistasis between *drl1* and *drl2* was tested within each of the 25 families of the maize NAM population. First, a 1-Mb window around each gene was identified and 100 polymorphic SNPs for each family extracted from these windows. Each *drl1* SNP was then tested with each *drl2* SNP in linear models that included either just the two SNPs themselves or the SNPs plus an interaction (epistasis) term. The P value for epistasis was determined by performing a likelihood ratio test of the two models, and all pairwise interaction P values (10,000 total) were averaged to obtain a single mean P value. (Since linkage disequilibrium within each NAM family decays very slowly, all SNPs within the region are tagging the same locus. Averaging was done primarily to account for different levels of missing data among the SNPs that could bias the results.) The same procedure was then repeated with 100 random pairs of regions across the maize genome, where each pair had to be located on separate chromosomes and no region could be within 50 megabases of *drl1* or *drl1*. The results for these random regions form a null distribution, and comparing this distribution to the actual results from *drl1/drl2* yields an empirical P value of how frequently such a result would occur by chance.

Accession Numbers

Sequence data from this article can be found in the GenBank/EMBL libraries under the following accession numbers:maize: *yab1*, GRMZM2G054795; *drl1*, GRMZM2G088309; *yab3*, GRMZM2G106204; *yab4*, GRMZM2G046829; *yab5*, GRMZM2G116646; *yab6*, GRMZM2G074124; *drl2*, GRMZM2G102218; *yab8*, GRMZM2G529859; *yab9*, GRMZM2G074543; *yab10*, GRMZM2G167824; *yab11*, GRMZM2G141955; *yab12*, GRMZM2G085873; and *yab14*, GRMZM2G005353;rice: *DL*, LOC_Os03g11600.1; *yab1*, LOC_Os07g06620.1; *yab2*, LOC_Os03g44710.1; *yab3*, LOC_Os10g36420.1; *yab4*, LOC_Os02g42950.1; *yab5*, LOC_Os04g45330.1; *yab6*, LOC_Os12g42610.1; and *yab7*, LOC_Os07g38410.1;Arabidopsis: *CRC*, AT1G69180.1; *FIL/YAB1*, AT2G45190.1; *INO*, AT1G23420.1; *YAB2*, AT1G08465.1; *YAB3*, AT4G00180.1; and *YAB5*, AT2G26580.1.

Supplemental Data

Supplemental Figure 1. Architecture of the mature maize leaf.

Supplemental Figure 2. Mature phenotypes of field-grown plants.

Supplemental Figure 3. Phenotypes associated with *drl1-R; drl2-M*.

Supplemental Figure 4. Clear cell proliferation is regulated by the *drl* genes.

Supplemental Figure 5. Effects of *drl1-R* and *drl2-M* on the blade-sheath boundary.

Supplemental Figure 6. Genetic complementation tests among *drl1* alleles.

Supplemental Figure 7. Phenotypes of *drl1-Ds* single mutants and with *drl2-M*.

Supplemental Figure 8. Alignment of amino acid sequences encoded by *drl* alleles.

Supplemental Figure 9. *yab7* transcript levels in *drl2* natural variant and mutant alleles.

Supplemental Figure 10. The *drl2-DsD08* mutant allele enhances the effects of the *drl1-R* allele.

Supplemental Figure 11. Phylogenetic footprinting of *YABBY* regulatory regions in the Pooid and Panicoid grasses.

Supplemental Figure 12. RNA in situ hybridization of maize *PHABULOSA* and *CUP SHAPE COTYLEDON2* orthologs in shoot apices.

Supplemental Figure 13. Linkage disequilibrium around *drl1* and *drl2* and phenotypic variance explained by these loci.

Supplemental Figure 14. Digenic epistatic interactions between associations.

Supplemental Table 1. Published phenotypic data used in this study.

Supplemental Table 2. Primers used in this study.

Supplemental Data Set 1. Alleles for GWAS analysis.

Supplemental File 1. Alignment used for phylogenetic analysis.

ACKNOWLEDGMENTS

We thank Harry Horner and Tracey Stewart at the Iowa State University Bessey Microscopy Facility for assistance with scanning electron microscopy

Downloaded from https://academic.oup.com/plcell/article/29/7/1622/6099203 by U.S. Department of Justice user on 16 August 2022

and Pete Lelonek for plant care. We also thank Kokulapalan (Gokul) Wimalanathan for help with phylogenetic analysis. We thank the many undergraduate students, especially Emery Peyton and Charlie Beeler, for their help in our summer genetics nurseries, and Dustin Miller for assistance with genotyping. We thank Erin Irish for insightful comments on the manuscript and Mike Scanlon and Robyn Johnston for the *ZmCUC2* and *ZmPHB* in situ probes. This work was supported by The University of Georgia and the National Science Foundation IOS-1238014 (J.G.W.), by the USDA-ARS (P.J.B. and E.S.B), and by the National Science Foundation (IOS-1238202 to E.V.).

AUTHOR CONTRIBUTIONS

J.S. designed research. J.S., J.G.W., E.U.-W., S.B., and E.V. performed research. P.J.B and E.S.B. contributed analytical tools. J.S., J.G.W., E.U.-W., and E.V. analyzed data. J.S. and E.V. wrote the article with input from all authors.

Received June 15, 2016; revised June 12, 2017; accepted July 7, 2017; published July 11, 2017.

REFERENCES

Alvarez, J., and Smyth, D.R. (1999). *CRABS CLAW* and *SPATULA*, two *Arabidopsis* genes that control carpel development in parallel with *AGAMOUS*. Development **126:** 2377–2386.

Becraft, P.W., Bongard-Pierce, D.K., Sylvester, A.W., Poethig, R.S., and Freeling, M. (1990). The liguleless-1 gene acts tissue specifically in maize leaf development. Dev. Biol. **141:** 220–232.

Becraft, P.W., and Freeling, M. (1991). Sectors of liguleless-1 tissue interrupt an inductive signal during maize leaf development. Plant Cell **3:** 801–807.

Bell, E.M., Lin, W.C., Husbands, A.Y., Yu, L., Jaganatha, V., Jablonska, B., Mangeon, A., Neff, M.M., Girke, T., and Springer, P.S. (2012). Arabidopsis lateral organs boundaries negatively regulates brassinosteroid accumulation to limit growth in organ boundaries. Proc. Natl. Acad. Sci. USA **109:** 21146–21151.

Bennetzen, J.L., and Freeling, M. (1993). Grasses as a single genetic system: genome composition, collinearity and compatibility. Trends Genet. **9:** 259–261.

Bosabalidis, A.M., Evert, R.F., and Russin, W.A. (1994). Ontogeny of the vascular bundles and contiguous tissues of the maize leaf blade. Am. J. Bot. **81:** 745–752.

Boter, M., Golz, J.F., Giménez-Ibañez, S., Fernandez-Barbero, G., Franco-Zorrilla, J.M., and Solano, R. (2015). FILAMENTOUS FLOWER is a direct target of JAZ3 and modulates responses to jasmonate. Plant Cell **27:** 3160–3174.

Bowman, J.L., and Smyth, D.R. (1999). *CRABS CLAW*, a gene that regulates carpel and nectary development in *Arabidopsis*, encodes a novel protein with zinc finger and helix-loop-helix domains. Development **126:** 2387–2396.

Brooks III, L., et al. (2009). Microdissection of shoot meristem functional domains. PLoS Genet. **5:** e1000476.

Buckler, E.S., et al. (2009). The genetic architecture of maize flowering time. Science **325:** 714–718.

Cao, H., and Chen, S. (1993). Brassinosteroid-induced rice lamina joint inclination and its relation to indole-3-acetic acid and ethylene. Plant Growth Regul. **16:** 189–196.

Chen, Q., Atkinson, A., Otsuga, D., Christensen, T., Reynolds, L., and Drews, G.N. (1999). The Arabidopsis *FILAMENTOUS FLOWER* gene is required for flower formation. Development **126:** 2715–2726.

Chen, W., VanOpdorp, N., Fitzl, D., Tewari, J., Friedemann, P., Greene, T., Thompson, S., Kumpatla, S., and Zheng, P. (2012). Transposon insertion in a cinnamyl alcohol dehydrogenase gene is responsible for a brown midrib1 mutation in maize. Plant Mol. Biol. **80:** 289–297.

Chia, J.-M., et al. (2012). Maize HapMap2 identifies extant variation from a genome in flux. Nat. Genet. **44:** 803–807.

Clouse, S.D. (2011). Brassinosteroid signal transduction: from receptor kinase activation to transcriptional networks regulating plant development. Plant Cell **23:** 1219–1230.

Clouse, S.D., and Sasse, J.M. (1998). BRASSINOSTEROIDS: Essential regulators of plant growth and development. Annu. Rev. Plant Physiol. Plant Mol. Biol. **49:** 427–451.

Duncan, W.G. (1971). Leaf angle, leaf area, and canopy photosynthesis. Crop Sci. **11:** 482–485.

Duvick, D.N. (2005). Genetic progress in yield of United States maize (*Zea mays* L.). Maydica **50:** 193–202.

Elshire, R.J., Glaubitz, J.C., Sun, Q., Poland, J.A., Kawamoto, K., Buckler, E.S., and Mitchell, S.E. (2011). A robust, simple genotyping-by-sequencing (GBS) approach for high diversity species. PLoS One **6:** e19379.

Emery, J.F., Floyd, S.K., Alvarez, J., Eshed, Y., Hawker, N.P., Izhaki, A., Baum, S.F., and Bowman, J.L. (2003). Radial patterning of Arabidopsis shoots by class III HD-ZIP and KANADI genes. Curr. Biol. **13:** 1768–1774.

Eshed, Y., Izhaki, A., Baum, S.F., Floyd, S.K., and Bowman, J.L. (2004). Asymmetric leaf development and blade expansion in Arabidopsis are mediated by KANADI and YABBY activities. Development **131:** 2997–3006.

Floyd, S.K., and Bowman, J.L. (2007). The ancestral developmental tool kit of land plants. Int. J. Plant Sci. **168:** 1–35.

Freeling, M. (2009). Bias in plant gene content following different sorts of duplication: tandem, whole-genome, segmental, or by transposition. Annu. Rev. Plant Biol. **60:** 433–453.

Foster, T., Hay, A., Johnston, R., and Hake, S. (2004). The establishment of axial patterning in the maize leaf. Development **131:** 3921–3929.

Foster, T.M., and Timmermans, M. (2009). Axial patterning of the maize leaf. In Handbook of Maize: Its Biology J. Bennetzen and S. Hake, eds (New York: Springer), pp. 161–178.

Fowler, J.E., and Freeling, M. (1996). Genetic analysis of mutations that alter cell fates in maize leaves: dominant Liguleless mutations. Dev. Genet. **18:** 198–222.

Fowler, J.E., Muehlbauer, G.J., and Freeling, M. (1996). Mosaic analysis of the liguleless3 mutant phenotype in maize by coordinate suppression of mutator-insertion alleles. Genetics **143:** 489–503.

Frazer, K.A., Pachter, L., Poliakov, A., Rubin, E.M., and Dubchak, I. (2004). VISTA: computational tools for comparative genomics. Nucleic Acids Res. **32:** W273–W279.

Fu, Y., Emrich, S.J., Guo, L., Wen, T.J., Ashlock, D.A., Aluru, S., and Schnable, P.S. (2005). Quality assessment of maize assembled genomic islands (MAGIs) and large-scale experimental verification of predicted genes. Proc. Natl. Acad. Sci. USA **102:** 12282–12287.

Galinat, W. (1959). The phytomer in relation to the floral homologies in the American Maydea. Bot. Mus. Leafl. Harv. Univ. **19:** 1–32.

Gao, H., Smith, J., Yang, M., Jones, S., Djukanovic, V., Nicholson, M.G., West, A., Bidney, D., Falco, S.C., Jantz, D., and Lyznik, L.A. (2010). Heritable targeted mutagenesis in maize using a designed endonuclease. Plant J. **61:** 176–187.

Gaut, B.S., and Doebley, J.F. (1997). DNA sequence evidence for the segmental allotetraploid origin of maize. Proc. Natl. Acad. Sci. USA **94:** 6809–6814.

Gendron, J.M., Liu, J.S., Fan, M., Bai, M.Y., Wenkel, S., Springer, P.S., Barton, M.K., and Wang, Z.Y. (2012). Brassinosteroids regulate

Downloaded from https://academic.oup.com/plcell/article/29/7/1622/6099203 by U.S. Department of Justice user on 16 August 2022

organ boundary formation in the shoot apical meristem of *Arabidopsis*. Proc. Natl. Acad. Sci. USA **109:** 21152–21157.

Goldshmidt, A., Alvarez, J.P., Bowman, J.L., and Eshed, Y. (2008). Signals derived from YABBY gene activities in organ primordia regulate growth and partitioning of Arabidopsis shoot apical meristems. Plant Cell **20:** 1217–1230.

Golz, J.F., Roccaro, M., Kuzoff, R., and Hudson, A. (2004). GRAMINIFOLIA promotes growth and polarity of Antirrhinum leaves. Development **131:** 3661–3670.

Gore, M.A., Chia, J.-M., Elshire, R.J., Sun, Q., Ersoz, E.S., Hurwitz, B.L., Peiffer, J.A., McMullen, M.D., Grills, G.S., Ross-Ibarra, J., Ware, D.H., and Buckler, E.S. (2009). A first-generation haplotype map of maize. Science **326:** 1115–1117.

Gray, J., et al. (2009). A recommendation for naming transcription factor proteins in the grasses. Plant Physiol. **149:** 4–6.

Hartwig, T., Chuck, G.S., Fujioka, S., Klempien, A., Weizbauer, R., Potluri, D.P.V., Choe, S., Johal, G.S., and Schulz, B. (2011). Brassinosteroid control of sex determination in maize. Proc. Natl. Acad. Sci. USA **108:** 19814–19819.

Hay, A., and Hake, S. (2004). The dominant mutant *Wavy auricle in blade1* disrupts patterning in a lateral domain of the maize leaf. Plant Physiol. **135:** 300–308.

Hong, Z., et al. (2002). Loss-of-function of a rice brassinosteroid biosynthetic enzyme, C-6 oxidase, prevents the organized arrangement and polar elongation of cells in the leaves and stem. Plant J. **32:** 495–508.

Huelsenbeck, J.P., and Ronquist, F. (2001). MRBAYES: Bayesian inference of phylogenetic trees. Bioinformatics **17:** 754–755.

Irish, E.E., and Jegla, D. (1997). Regulation of extent of vegetative development of the maize shoot meristem. Plant J. **11:** 63–71.

Irish, E.E., and Karlen, S. (1998). Restoration of juvenility in maize shoots by meristem culture. Int. J. Plant Sci. **159:** 695–701.

Irish, E.E., and Nelson, T.M. (1988). Development of maize plants from cultured shoot apices. Planta **175:** 9–12.

Ishikawa, M., Ohmori, Y., Tanaka, W., Hirabayashi, C., Murai, K., Ogihara, Y., Yamaguchi, T., and Hirano, H.-Y. (2009). The spatial expression patterns of *DROOPING LEAF* orthologs suggest a conserved function in grasses. Genes Genet. Syst. **84:** 137–146.

Jackson, D., Veit, B., and Hake, S. (1994). Expression of maize *KNOTTED1* related homeobox genes in the shoot apical meristem predicts patterns of morphogenesis in the vegetative shoot. Development **120:** 405–413.

Javelle, M., Marco, C.F., and Timmermans, M. (2011). In situ hybridization for the precise localization of transcripts in plants. J. Vis. Exp. **57:** e3328.

Je, B.I., et al. (2016). Signaling from maize organ primordia via FASCIATED EAR3 regulates stem cell proliferation and yield traits. Nat. Genet. **48:** 785–791.

Jeanmougin, F., Thompson, J.D., Gouy, M., Higgins, D.G., and Gibson, T.J. (1998). Multiple sequence alignment with Clustal X. Trends Biochem. Sci. **23:** 403–405.

Johnston, R., Leiboff, S., and Scanlon, M.J. (2015). Ontogeny of the sheathing leaf base in maize (*Zea mays*). New Phytol. **205:** 306–315.

Johnston, R., Wang, M., Sun, Q., Sylvester, A.W., Hake, S., and Scanlon, M.J. (2014). Transcriptomic analyses indicate that maize ligule development recapitulates gene expression patterns that occur during lateral organ initiation. Plant Cell **26:** 4718–4732.

Juarez, M.T., Kui, J.S., Thomas, J., Heller, B.A., and Timmermans, M.C. (2004a). microRNA-mediated repression of rolled leaf1 specifies maize leaf polarity. Nature **428:** 84–88.

Juarez, M.T., Twigg, R.W., and Timmermans, M.C. (2004b). Specification of adaxial cell fate during maize leaf development. Development **131:** 4533–4544.

Katoh, K., and Toh, H. (2010). Parallelization of the MAFFT multiple sequence alignment program. Bioinformatics **26:** 1899–1900.

Kiesselbach, T. (1949). The Structure and Reproduction of Corn. (Lincoln, NE: University of Nebraska College of Agriculture).

Kir, G., Ye, H., Nelissen, H., Neelakandan, A.K., Kusnandar, A.S., Luo, A., Inzé, D., Sylvester, A.W., Yin, Y., and Becraft, P.W. (2015). RNA interference knockdown of BRASSINOSTEROID INSENSITIVE1 in maize reveals novel functions for brassinosteroid signaling in controlling plant architecture. Plant Physiol. **169:** 826–839.

Kump, K.L., Bradbury, P.J., Wisser, R.J., Buckler, E.S., Belcher, A.R., Oropeza-Rosas, M.A., Zwonitzer, J.C., Kresovich, S., McMullen, M.D., Ware, D., Balint-Kurti, P.J., and Holland, J.B. (2011). Genome-wide association study of quantitative resistance to southern leaf blight in the maize nested association mapping population. Nat. Genet. **43:** 163–168.

Lambert, R.J., and Johnston, R.R. (1978). Leaf angle, tassel morphology, and the performance of maize hybrids. Crop Sci. **18:** 499–502.

Lamoreaux, R.J., Chaney, W.R., and Brown, K.M. (1978). The plastochron index: a review after two decades of use. Am. J. Bot. **65:** 586–593.

Laudencia-Chingcuanco, D., and Hake, S. (2002). The *indeterminate floral apex1* gene regulates meristem determinacy and identity in the maize inflorescence. Development **129:** 2629–2638.

Li, Y., Segal, G., Wang, Q., and Dooner, H.K. (2013). Gene tagging with engineered Ds elements in maize. Methods Mol. Biol. **1057:** 83–99.

Liu, S., Chen, H.D., Makarevitch, I., Shirmer, R., Emrich, S.J., Dietrich, C.R., Barbazuk, W.B., Springer, N.M., and Schnable, P.S. (2010). High-throughput genetic mapping of mutants via quantitative single nucleotide polymorphism typing. Genetics **184:** 19–26.

Makarevitch, I., Thompson, A., Muehlbauer, G.J., and Springer, N.M. (2012). Brd1 gene in maize encodes a brassinosteroid C-6 oxidase. PLoS One **7:** e30798.

McConnell, J.R., Emery, J., Eshed, Y., Bao, N., Bowman, J., and Barton, M.K. (2001). Role of *PHABULOSA* and *PHAVOLUTA* in determining radial patterning in shoots. Nature **411:** 709–713.

McDaniel, C.N., and Poethig, R.S. (1988). Cell-lineage patterns in the shoot apical meristem of the germinating maize embryo. Planta **175:** 13–22.

McMullen, M.D., et al. (2009). Genetic properties of the maize nested association mapping population. Science **325:** 737–740.

Michelmore, R.W., Paran, I., and Kesseli, R.V. (1991). Identification of markers linked to disease-resistance genes by bulked segregant analysis: a rapid method to detect markers in specific genomic regions by using segregating populations. Proc. Natl. Acad. Sci. USA **88:** 9828–9832.

Moon, J., Candela, H., and Hake, S. (2013). The Liguleless narrow mutation affects proximal-distal signaling and leaf growth. Development **140:** 405–412.

Moore, G., Devos, K.M., Wang, Z., and Gale, M.D. (1995). Cereal genome evolution. Grasses, line up and form a circle. Curr. Biol. **5:** 737–739.

Moreno, M.A., Harper, L.C., Krueger, R.W., Dellaporta, S.L., and Freeling, M. (1997). liguleless1 encodes a nuclear-localized protein required for induction of ligules and auricles during maize leaf organogenesis. Genes Dev. **11:** 616–628.

Muehlbauer, G.J., Fowler, J.E., and Freeling, M. (1997). Sectors expressing the homeobox gene liguleless3 implicate a time-dependent mechanism for cell fate acquisition along the proximal-distal axis of the maize leaf. Development **124:** 5097–5106.

Muehlbauer, G.J., Fowler, J.E., Girard, L., Tyers, R., Harper, L., and Freeling, M. (1999). Ectopic expression of the maize homeobox gene liguleless3 alters cell fates in the leaf. Plant Physiol. **119:** 651–662.

Downloaded from https://academic.oup.com/plcell/article/29/7/1622/6099203 by U.S. Department of Justice user on 16 August 2022

Nagasawa, N., Miyoshi, M., Sano, Y., Satoh, H., Hirano, H., Sakai, H., and Nagato, Y. (2003). *SUPERWOMAN1* and *DROOPING LEAF* genes control floral organ identity in rice. Development **130:** 705–718.

Navarro, C., Efremova, N., Golz, J.F., Rubiera, R., Kuckenberg, M., Castillo, R., Tietz, O., Saedler, H., and Schwarz-Sommer, Z. (2004). Molecular and genetic interactions between STYLOSA and GRAMINIFOLIA in the control of Antirrhinum vegetative and reproductive development. Development **131:** 3649–3659.

Ohmori, Y., Abiko, M., Horibata, A., and Hirano, H.-Y. (2008). A transposon, *Ping*, is integrated into intron 4 of the *DROOPING LEAF* gene of rice, weakly reducing its expression and causing a mild drooping leaf phenotype. Plant Cell Physiol. **49:** 1176–1184.

Ohmori, Y., Toriba, T., Nakamura, H., Ichikawa, H., and Hirano, H.-Y. (2011). Temporal and spatial regulation of *DROOPING LEAF* gene expression that promotes midrib formation in rice. Plant J. **65:** 77–86.

Osmont, K.S., Jesaitis, L.A., and Freeling, M. (2003). The *extended auricle1* (*eta1*) gene is essential for the genetic network controlling postinitiation maize leaf development. Genetics **165:** 1507–1519.

Peiffer, J.A., Flint-Garcia, S.A., De Leon, N., McMullen, M.D., Kaeppler, S.M., and Buckler, E.S. (2013). The genetic architecture of maize stalk strength. PLoS One **8:** e67066.

Peiffer, J.A., Romay, M.C., Gore, M.A., Flint-Garcia, S.A., Zhang, Z., Millard, M.J., Gardner, C.A., McMullen, M.D., Holland, J.B., Bradbury, P.J., and Buckler, E.S. (2014). The genetic architecture of maize height. Genetics **196:** 1337–1356.

Pendleton, J.W., Smith, G.E., Winter, S.R., and Johnston, T.J. (1968). Field investigations of the relationships of leaf angle in corn (*Zea mays* L.) to grain yield and apparent photosynthesis. Agron. J. **60:** 422–424.

Pepper, G.E., Pearce, R.B., and Mock, J.J. (1977). Leaf orientation and yield of maize. Crop Sci. **17:** 883–886.

Poethig, R.S. (2013). Vegetative phase change and shoot maturation in plants. Curr. Top. Dev. Biol. **105:** 125–152.

Poland, J.A., Bradbury, P.J., Buckler, E.S., and Nelson, R.J. (2011). Genome-wide nested association mapping of quantitative resistance to northern leaf blight in maize. Proc. Natl. Acad. Sci. USA **108:** 6893–6898.

Romay, M.C., et al. (2013). Comprehensive genotyping of the USA national maize inbred seed bank. Genome Biol. **14:** R55.

Russell, S.H., and Evert, R.F. (1985). Leaf vasculature in *Zea mays* L. Planta **164:** 448–458.

Sarojam, R., Sappl, P.G., Goldshmidt, A., Efroni, I., Floyd, S.K., Eshed, Y., and Bowman, J.L. (2010). Differentiating *Arabidopsis* shoots from leaves by combined YABBY activities. Plant Cell **22:** 2113–2130.

Sawa, S., Watanabe, K., Goto, K., Liu, Y.G., Shibata, D., Kanaya, E., Morita, E.H., and Okada, K. (1999). *FILAMENTOUS FLOWER*, a meristem and organ identity gene of Arabidopsis, encodes a protein with a zinc finger and HMG-related domains. Genes Dev. **13:** 1079–1088.

Scanlon, M.J., Schneeberger, R.G., and Freeling, M. (1996). The maize mutant *narrow sheath* fails to establish leaf margin identity in a meristematic domain. Development **122:** 1683–1691.

Schnable, J.C. (2015). Genome evolution in maize: from genomes back to genes. Annu. Rev. Plant Biol. **66:** 329–343.

Schnable, J.C., Springer, N.M., and Freeling, M. (2011). Differentiation of the maize subgenomes by genome dominance and both ancient and ongoing gene loss. Proc. Natl. Acad. Sci. USA **108:** 4069–4074.

Sharman, B.C. (1942). Developmental anatomy of the shoot of *Zea mays* L. Ann. Bot. (Lond.) **6:** 245–282.

Siegfried, K.R., Eshed, Y., Baum, S.F., Otsuga, D., Drews, G.N., and Bowman, J.L. (1999). Members of the *YABBY* gene family specify abaxial cell fate in *Arabidopsis.* Development **126:** 4117–4128.

Skinner, M.E., Uzilov, A.V., Stein, L.D., Mungall, C.J., and Holmes, I.H. (2009). JBrowse: a next-generation genome browser. Genome Res. **19:** 1630–1638.

Snow, R. (1929). The young leaf as the inhibiting organ. New Phytol. **28:** 345–348.

Stahle, M.I., Kuehlich, J., Staron, L., von Arnim, A.G., and Golz, J.F. (2009). YABBYs and the transcriptional corepressors LEUNIG and LEUNIG_HOMOLOG maintain leaf polarity and meristem activity in *Arabidopsis.* Plant Cell **21:** 3105–3118.

Sun, S., Chen, D., Li, X., Qiao, S., Shi, C., Li, C., Shen, H., and Wang, X. (2015). Brassinosteroid signaling regulates leaf erectness in *Oryza sativa* via the control of a specific U-type cyclin and cell proliferation. Dev. Cell **34:** 220–228.

Sylvester, A.W., Cande, W.Z., and Freeling, M. (1990). Division and differentiation during normal and *liguleless-1* maize leaf development. Development **110:** 985–1000.

Tanaka, W., Toriba, T., Ohmori, Y., Yoshida, A., Kawai, A., Mayama-Tsuchida, T., Ichikawa, H., Mitsuda, N., Ohme-Takagi, M., and Hirano, H.-Y. (2012). The *YABBY* gene *TONGARI-BOUSHI1* is involved in lateral organ development and maintenance of meristem organization in the rice spikelet. Plant Cell **24:** 80–95.

Tang, H.M., Liu, S., Hill-Skinner, S., Wu, W., Reed, D., Yeh, C.-T., Nettleton, D., and Schnable, P.S. (2014). The maize *brown midrib2* (*bm2*) gene encodes a methylenetetrahydrofolate reductase that contributes to lignin accumulation. Plant J. **77:** 380–392.

Tian, F., Bradbury, P.J., Brown, P.J., Hung, H., Sun, Q., Flint-Garcia, S., Rocheford, T.R., McMullen, M.D., Holland, J.B., and Buckler, E.S. (2011). Genome-wide association study of leaf architecture in the maize nested association mapping population. Nat. Genet. **43:** 159–162.

Tong, H., Liu, L., Jin, Y., Du, L., Yin, Y., Qian, Q., Zhu, L., and Chu, C. (2012). DWARF AND LOW-TILLERING acts as a direct downstream target of a GSK3/SHAGGY-like kinase to mediate brassinosteroid responses in rice. Plant Cell **24:** 2562–2577.

Toriba, T., Harada, K., Takamura, A., Nakamura, H., Ichikawa, H., Suzaki, T., and Hirano, H.-Y. (2007). Molecular characterization the *YABBY* gene family in *Oryza sativa* and expression analysis of *OsYABBY1.* Mol. Genet. Genomics **277:** 457–468.

Tsuda, K., Kurata, N., Ohyanagi, H., and Hake, S. (2014). Genome-wide study of KNOX regulatory network reveals brassinosteroid catabolic genes important for shoot meristem function in rice. Plant Cell **26:** 3488–3500.

Valdar, W., Holmes, C.C., Mott, R., and Flint, J. (2009). Mapping in structured populations by resample model averaging. Genetics **182:** 1263–1277.

Vollbrecht, E., et al. (2010). Genome-wide distribution of transposed Dissociation elements in maize. Plant Cell **22:** 1667–1685.

Wada, K., Marumo, S., Ikekawa, N., Morisaki, M., and Mori, K. (1981). Brassinolide and homobrassinolide promotion of lamina inclination of rice seedlings. Plant Cell Physiol. **22:** 323–325.

Wallace, J.G., Bradbury, P.J., Zhang, N., Gibon, Y., Stitt, M., and Buckler, E.S. (2014a). Association mapping across numerous traits reveals patterns of functional variation in maize. PLoS Genet. **10:** e1004845.

Wallace, J.G., Larsson, S.J., and Buckler, E.S. (2014b). Entering the second century of maize quantitative genetics. Heredity (Edinb) **112:** 30–38.

Walsh, J., Waters, C.A., and Freeling, M. (1998). The maize gene *liguleless2* encodes a basic leucine zipper protein involved in the establishment of the leaf blade-sheath boundary. Genes Dev. **12:** 208–218.

Wang, Z.Y., Bai, M.Y., Oh, E., and Zhu, J.Y. (2012). Brassinosteroid signaling network and regulation of photomorphogenesis. Annu. Rev. Genet. **46:** 701–724.

Woodward, J.B., Abeydeera, N.D., Paul, D., Phillips, K., Rapala-Kozik, M., Freeling, M., Begley, T.P., Ealick, S.E., McSteen, P., and Scanlon, M.J. (2010). A maize thiamine auxotroph is defective in shoot meristem maintenance. Plant Cell **22:** 3305–3317.

Downloaded from https://academic.oup.com/plcell/article/29/7/1622/6099203 by U.S. Department of Justice user on 16 August 2022

Yamaguchi, T., Nagasawa, N., Kawasaki, S., Matsuoka, M., Nagato, Y., and Hirano, H.-Y. (2004). The YABBY gene *DROOPING LEAF* regulates carpel specification and midrib development in *Oryza sativa.* Plant Cell **16:** 500–509.

Yamamuro, C., Ihara, Y., Wu, X., Noguchi, T., Fujioka, S., Takatsuto, S., Ashikari, M., Kitano, H., and Matsuoka, M. (2000). Loss of function of a rice brassinosteroid insensitive1 homolog prevents internode elongation and bending of the lamina joint. Plant Cell **12:** 1591–1606.

Yilmaz, A., Nishiyama, M.Y., Jr., Fuentes, B.G., Souza, G.M., Janies, D., Gray, J., and Grotewold, E. (2009). GRASSIUS: a platform for comparative regulatory genomics across the grasses. Plant Physiol. **149:** 171–180.

Zhang, L.Y., et al. (2009). Antagonistic HLH/bHLH transcription factors mediate brassinosteroid regulation of cell elongation and plant development in rice and Arabidopsis. Plant Cell **21:** 3767–3780.

Zhang, N., et al. (2015). Genome-wide association of carbon and nitrogen metabolism in the maize nested association mapping population. Plant Physiol. **168:** 575–583.

Downloaded from https://academic.oup.com/plcell/article/29/7/1622/6099203 by U.S. Department of Justice user on 16 August 2022